HZDR-076

TWO-PHASE FLOW EXPERIMENTS ON COUNTER-CURRENT FLOW LIMITATION IN A MODEL OF THE HOT LEG OF A PRESSURIZED WATER REACTOR (2015 TEST SERIES)

Matthias Beyer, Dirk Lucas, Heiko Pietruske, Lutz Szalinski

WISSENSCHAFTLICH-TECHNISCHE BERICHTE

HZDR

HELMHOLTZ
ZENTRUM DRESDEN
ROSSENDORF

Matthias Beyer, Dirk Lucas,
Heiko Pietruske, Lutz Szalinski

TWO-PHASE FLOW EXPERIMENTS ON COUNTER-CURRENT FLOW LIMITATION IN A MODEL OF THE HOT LEG OF A PRESSURIZED WATER REACTOR (2015 TEST SERIES)

HZDR

HELMHOLTZ
ZENTRUM DRESDEN
ROSSENDORF

Technischer Fachbericht

Experimente an Zweiphasenströmungen mit Gegenstrombegrenzung im Heißstrangmodel eines Druckwasserreaktors

Technical Report

Two-Phase Flow Experiments on Counter-Current Flow Limitation in a Model of the Hot Leg of a Pressurized Water Reactor

Vorhabenstitel: **TOPFLOW-Experimente, Modellentwicklung und Validierung zur Qualifizierung von CFD-Codes für Zweiphasenströmungen**

Project Title: **TOPFLOW experiments, development and validation of models qualifying of CFD codes for two-phase flows**

Autoren / Author(s): **M. Beyer, D. Lucas, H. Pietruske, L. Szalinski**

Dienststelle der Autoren / **Helmholtz-Zentrum Dresden-Rossendorf**
Performing Organisation: **Institut für Sicherheitsforschung**

Gefördert durch:

Bundesministerium
für Wirtschaft
und Energie

aufgrund eines Beschlusses
des Deutschen Bundestages

Berichtsblatt

18. Kurzfassung

Die Gegenstrombegrenzung im Heißstrang eines Druckwasserreaktors ist bei verschiedenen Störfallszenarien, die mit einem Kühlmittelverlust verbunden sind, von Bedeutung. Aufbauend auf den Erfahrungen einer ersten Heißstrangmodell-Versuchsserie wurden Experimente zur stationären Gegenstrombegrenzung im TOPFLOW-Drucktank durchgeführt. Die Versuchsserie umfasst sowohl die Gegenstrombegrenzung für Luft-Wasser-Strömungen bei Drücken von 1 und 2 bar als auch Dampf-Wasser-Experimente bei 10, 25 und 50 bar. Bei den Experimenten erfolgten eine optische Beobachtung des gesamten Kanals, Druckmessungen entlang des horizontalen Teils und eine Bestimmung der Wasserspiegel im Reaktor- sowie im Dampferzeuger-Simulator.

Dieser Bericht dokumentiert den Versuchsaufbau, einschließlich der Beschreibung von Betriebs- und Spezialmesstechnik, die Versuchsdurchführung sowie die erhaltenen Daten.

Aus diesen Daten wurden die Flutkurven auf Basis der Wallis-Parameter berechnet. Diese zeigen eine leichte Verschiebung der Kurven in Abhängigkeit vom Druck. Außerdem wurde eine Abnahme des Anstiegs mit dem Druck gefunden. Weitere Untersuchungen betrafen Hysterese-Effekte sowie die Frequenzen der Flüssigkeitsschwälle, die eine Abhängigkeit vom Druck und vom eingespeisten Wassermassestrom zeigen.Die Daten stehen zur CFD-Modellentwicklung und –validierung zur Verfügung.

19. Schlagwörter
Experiment, CFD, Zweiphasenströmung, Gegenstrombegrenzung, Flutkurve, Schwallfrequenz

20. Verlag	21. Preis

Document Control Sheet

1. ISBN or ISSN Printed: 2191-8708 Electronic: 2191-8716	2. type of document Technical Report	
3. title Tow-Phase Flow Experiments on Counter-Current Flow Limitation in a Model of the Hot Leg of a Pressurized water Reactor		
4. author(s) (family name, first name(s)) M. Beyer, D. Lucas, H. Pietruske, L. Szalinski	5. end of project 31.12.2015	
	6. publication date December 2016	
	7. form of publication Booklet	
8. performing organization(s) (name, address) Helmholtz-Zentrum Dresden-Rossendorf Institut für Fluiddynamik Bautzner Landstr. 400 01328 Dresden	9. originator's report no. HZDR-076	
	10. reference no. 150 1411	
	11. no. of pages 63	
13. sponsoring agency (name, address) Federal Ministry for Economic Affairs and Energy (BMWi) 11019 Berlin	12. no. of references 7	
	14. no. of tables 3	
	no. of figures 22	
16. supplementary notes		
17. presented at (title, place, date)		

18. abstract

Counter-Current Flow Limitation (CCFL) is of importance for PWR safety analyses in several accident scenarios connected with loss of coolant. Basing on the experiences obtained during a first series of hot leg tests now new experiments on counter-current flow limitation were conducted in the TOPFLOW pressure vessel. The test series comprises air-water tests at 1 and 2 bar as well as steam-water tests at 10, 25 and 50 bar. During the experiments the flow structure was observed along the hot leg model using a high-speed camera and web-cams. In addition pressure was measured at several positions along the horizontal part and the water levels in the reactor-simulator and steam-generator-simulator tanks were determined.

This report documents the experimental setup including the description of operational and special measuring techniques, the experimental procedure and the data obtained.

From these data flooding curves were obtained basing on the Wallis parameter. The results show a slight shift of the curves in dependency of the pressure. In addition a slight decrease of the slope was found with increasing pressure. Additional investigations concern the effects of hysteresis and the frequencies of liquid slugs. The latter ones show a dependency on pressure and the mass flow rate of the injected water.

The data are available for CFD-model development and validation.

19. keywords experiment, CFD, two-phase flow, counter-current flow limitation, flooding characteristic, slug frequency		
20. publisher	21. price	

Content

Appendices (as pdf-files)

App. 1 Technical drawings of the CCFL test rig

App. 2 Technical information sheet of Borofloat 33 glass panes

App. 3 Data sheet of the LED illumination panels BacklightMatrix V2

List of abbreviation

CCF	Counter-Current Flow
CCFL	Counter-Current Flow Limitation
CFD	Computational Fluid Dynamics
DENISE	Direct Condensation and Entrainment Installation for Steam Experiments
HZDR	Helmholtz-Zentrum Dresden-Rossendorf e.V.
ISA	International Federation of the National Standardizing Associations
LED	Light-emitting diode
LOCA	Loss of coolant accident
NPP	Nuclear Power Plant
OPC	Open Platform Communications
PCS	Process control system @ TOPFLOW
PWR	Pressurized Water Reactor
RPV	Reactor Pressure Vessel
SG	Steam generator
TOPFLOW	Transient two phase flow test facility

Physical value

A	cross section area, area
α	heat transfer coefficient
β	coefficient of thermal expansion
c_p	isobaric specific heat capacity
Δ	difference
F	frequency
FFT	Fast Fourier Transformation
g	gravitational acceleration
Gr	Grashof number
H	height
h	enthalpy
j	superficial velocity
j*	non-dimensional superficial velocity
k	coefficient
L	level, length
l	length
λ	thermal conductivity
M	molar mass
m	mass flow, mass
ν	kinematic viscosity
Nu	Nusselt number

p	pressure
Pr	Prandtl number
Q	heat flux
ρ	density
R	Universal Gas Constant
r	radius
R^2	coefficient of determination
Ra	Rayleigh number
RO	rate of occurrence
t	temperature [°C]
T	temperature [K]
τ	time
V	volume flow, volume
W	width
xw	humidity
z	altitude

Indices

0	see level, start condition
1	start
2	end
air	air
at	atmospheric
av	averaged
cap	capacity
circ	circulation
ch	channel, characteristic
cond	condensation
cor, c	corrected
cs	cross section
cw	cooling water
cyl	cylinder
dis	discharged
G	gas
h	horizontal
i	inlet
in	inner
inc	inclined
imp	impulse pipe
k	phase selection
L	liquid
meas	measurement
N	noise
N2	nitrogen
norm	normative condition (p = 1.01325 bar and t = 273.15 K)
o	outlet
out	outer
pipe	pipe
ps	pressure sensor
rel	released

s	saturation
t	temperature-dependent
tank	tank
tr	test rig
trans	transport
TS	test section
w	weighted

1. Introduction

This report describes the counter-current flow limitation (CCFL) experiments conducted in the frame of the project "TOPFLOW-experiments, model development and validation for the qualification of CFD-codes for two-phase flow", funded by the German Federal Ministry for Economic Affairs and Energy (project number: 1501411). This work was a continuation of a CCFL test series done in frame of a previous TOPFLOW project.

The counter-current flow limitation phenomenon is relevant for the assessment of accident scenarios in pressurized water reactors (PWR). In the event of a loss-of coolant accident (LOCA) it is necessary to guarantee a safe removal of the decay-heat after shut-down of the Nuclear Power Plant (NPP). During loss of coolant accident the coolant inventory in the Primary loop leaks out and the level in the reactor pressure vessel decreases. Thus, a situation may occur that the main circulation pipes are partly or completely free of coolant. A natural circulation starts and steam from the reactor core flows along the hot leg pipe into the inlet chamber of a vertical steam generator (SG) and forward to the u-tubes (see Fig. 1). If the steam
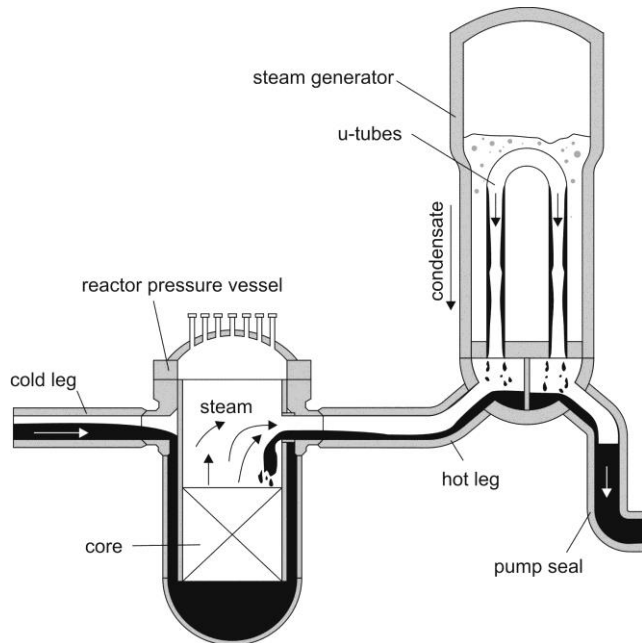
Fig. 1   Scheme of the Primary loop during reflux condenser mode

generator tank (secondary side) is still filled with feeding water, the steam at the primary side of the u-tubes condenses and the condensate returns again to the reactor pressure vessel using both pipes: the hot leg and the cold leg. Thereby the condensate in the hot leg flows in counter-current direction to the steam. A so-called reflux condenser mode may establish. In principle this scenario is very useful, because it transports heat from the reactor core to the secondary side of the SG without additional loss of coolant. If this process works very intensely, the high steam flow starts to restrain the condensate flow in the hot leg. This is the beginning of a counter-current flow limitation that may limit the heat transport to the secondary side. A detailed description of the reflux condenser mode in consideration with theoretical foundations and an analysis of previous activities of this effect were given in the technical report of the TOPFLOW-II project [1].

Many different co-current and counter-current gas-liquid flows and flows without water circulation were investigated in the frame of the previous TOPFLOW project. The evaluation and analysis of the previous data resulted in additional requirements of CCFL measurements, because only few CCFL tests were made and their boundary condition was not optimally. The test section consisted of a horizontal part, connected to a special inclined geometry module, that model the SG inlet chamber. Thereby the horizontal part was covered with non-transparent steel sheets that were slightly distorted during commissioning tests. Furthermore 2 rectangular adapters were mounted between the test section and each separation tank that lead to

unrealistic flow effects near the RPV- and the SG-simulators. Both simulator tanks were manufactured with stiffening brackets inside that resulted in difficulties in level balances. Also inside the test section little edges leaded to undesired slight flow turbulences.

In 2007 during the implementation of the TOPFLOW-II hot leg tests no circulation loops were installed on the TOPFLOW pressure tank. So the water flowed directly from the TOPFLOW steam generator circuitry to the SG simulator tank and was released from the RPV simulator to the TOPFLOW blow-off tank. This configuration allowed only water mass flows up to 1 kg/s that limited the test matrix. Furthermore the gas volume flow was increased stepwise up to zero penetration condition (flooding process) and then decreased also stepwise down to the end of CCFL. This operational procedure leaded to non-steady state condition that made the data evaluation difficult and resulted in relatively big deviations between the single test points of the flooding characteristic.

An additional disadvantage of the TOPFLOW-II experiments arose from the design of the SG simulator. The level in this tank increase continuously during the CCFL tests with constant injection of water into it. Hence the hydrostatic pressure in the SG simulator increased during the CCFL tests too that influenced the flow condition.

The steam CCFL tests in 2007 were made in a pressure range from 30 to 50 bar. Pressures less than 30 bar was not used due to the risk of the occurrence of water-hammers during the steam heat-up procedure. Nonetheless steam-water CCFL tests at less pressure are reasonable, because there are significant changes of the water and steam properties.

After the analysis of the high speed picture sequences of the TOPFLOW-II CCFL tests it was required that the horizontal channel has to be observed additional to the inclined part of the test section.

In consideration of the mentioned disadvantages of the previous CCFL tests it was decided to include a CCFL work package in the current TOPFLOW-III project to get more CFD grade data for code validation. In autumn 2013 the TOPFLOW team started to redesign and manufacture the new hot leg test section. After installation of the special measurement technique and commissioning of the test rig the measurements were done in June 2015. In the 2nd half year 2015 the data evaluation and analysis could be completed.

The present report describes in detail the design of the improved hot leg test section and his connection to the circulation loops of the TOPFLOW pressure tank and to the TOPFLOW facility. Then the operational and special measurement technique is explained. Further it gives an overview of the experimental procedure and the available data. The report closes with information about data processing procedures and first steps for analyzing the results.

2. Test section design and integration into the TOPFLOW facility

2.1 Construction

As aforementioned the current CCFL tests are a continuation of a previous test series. Nevertheless for clarity some important information about the background of the test rig design presented in the technical report [1] should be repeated in this paragraph. For the investigation of CCFL phenomena a model of a PWR of a German Konvoi type was chosen. The CCFL may appear in the hot leg and in the SG inlet chamber. So, these parts of the primary circuitry were modelled in a scale of 1:3. In order to provide optimal observation possibilities, the circular pipes were transformed into a flat, 50 mm wide geometry. This dimension was kept constant for the new tests. It was found as a good compromise between suppressing unwanted 3D flow features and having strong wall effects.

In the introduction a lot of disadvantages of the previous CCFL tests were specified. For this reason it was decided to redesign the horizontal test rig fundamentally to eliminate most of them. The rebuilding process included a complete new manufacturing of the basic components: RPV simulator tank, horizontal part of the hot leg, inclined model of the SG inlet chamber and SG separator tank. In principle only the platform was applied without changing. A basic advantage of the new test rig is a steel sheet that divides the SG separator tank in 2 parts: The first one serves as completion of the SG inlet chamber from the water side (B20A) and the second (B20B) is necessary to keep the level in the first constant, using the steel sheet as level drain. Thereby the height of the steel sheet was set to the upper bend of the inclined test section part (1097 mm). Fig. 2 shows a vertical cut through the mid-plane of the new CCFL test rig.
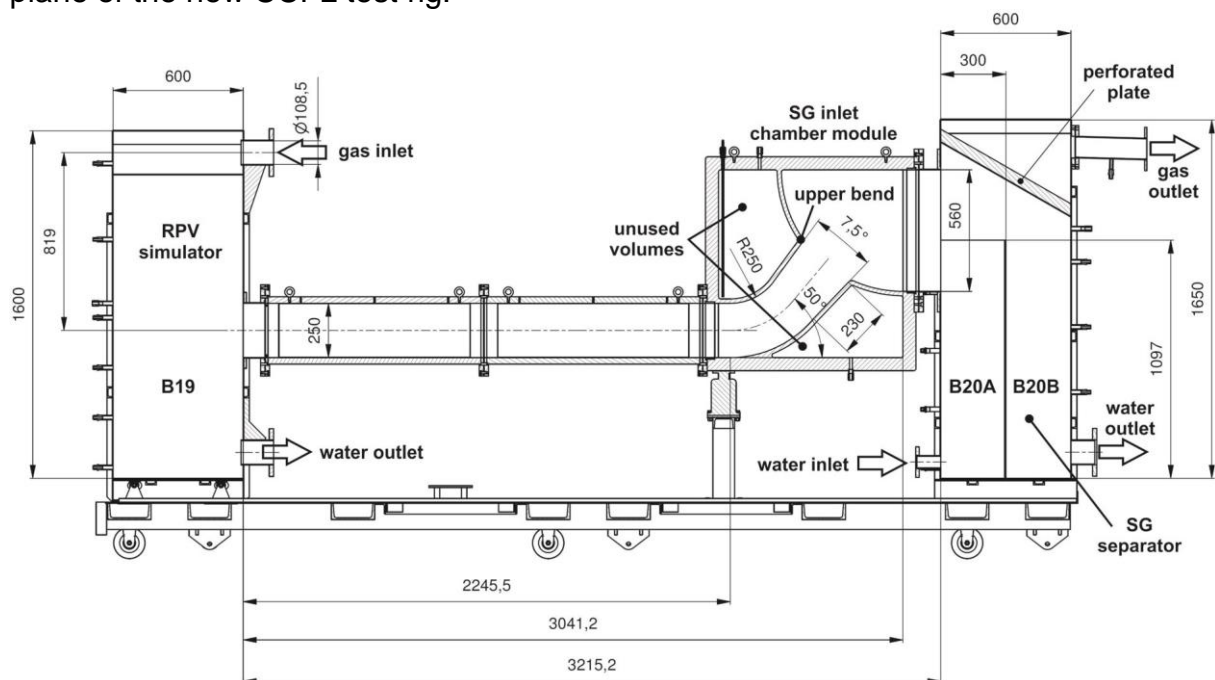
Fig. 2 Vertical cut through the CCFL test rig

Due to problems with the strong profiled glass pane mounted to the previous inclined SG inlet chamber module, the new design uses rectangular glass panes (889 x 874 mm²) that are fastened in separate steel frames. These frames are mounted to the basic module by bolted assembling and tightened by graphite seals. As illustrated in Fig. 2, two unused volumes remain in the left top and in the right bottom corner of the basic SG inlet chamber module due to the rectangular shape. To avoid

15

unaccepted stress around these volumes during pressure changes, both volumes are opened to the TOPFLOW pressure tank atmosphere. The distance between the glass panes and the curved steel wall limited the flow domain was sealed by PTFE tape (see Fig. 6).

The SG inlet chamber module is mounted to the separator tank. As aforementioned this tank consists of two parts: While the inner one (B20A) has a cross-section of 300 x 400 mm², the outer (B20B) is sized with 600 x 800 mm² and a height of 1.65 m. In the upper part of the tank a special perforated plate (Fig. 3) is fixed, that improves the separation of the very churn two-phase flow in the SG inlet chamber module. This is very important, because the data analysis requires an accurate mass balance in both tanks. Without the plate a significant amount of water drops may leave the SG separator tank and flow into the condenser. The middle part of the plate was manufactured without perforation, because the SG inlet chamber module was connected to the middle axis of the tank, so this area blocks the direct path of the fluid to the condenser.
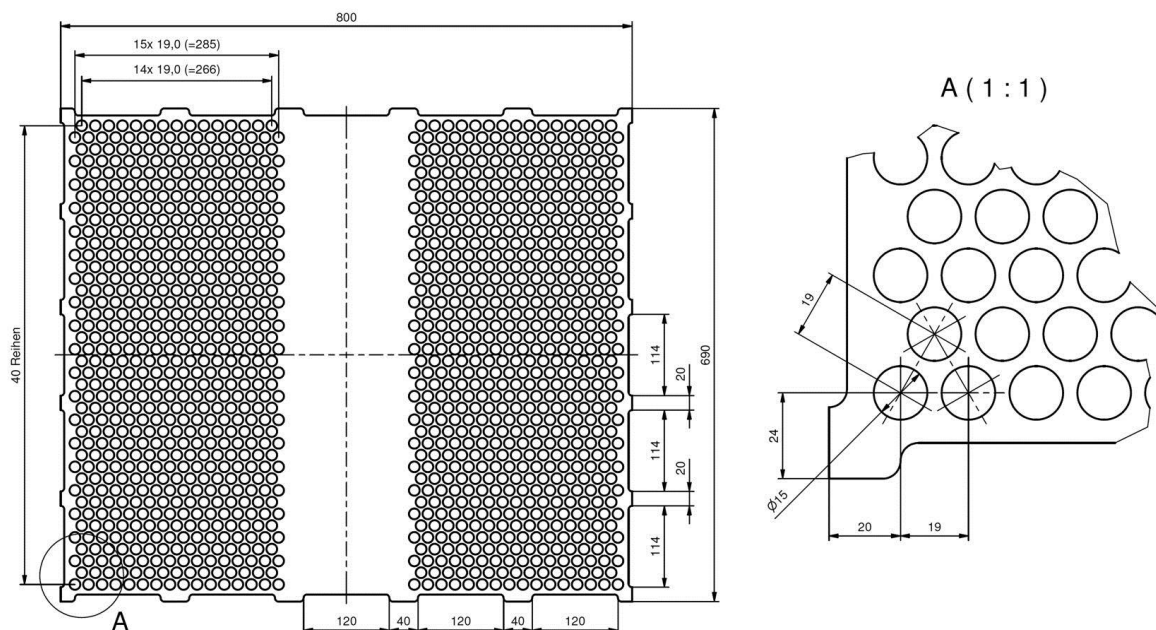
Fig. 3   Perforated plate mounted in the SG separator tank

Furthermore for an accurate mass balance the inner volumes of both tanks were designed with smooth walls and without inner stiffing details.

An additional improvement is the observation possibility at both horizontal test section segments. They also were equipped with 2 glass windows (901 x 268 mm²) each. The fixation was solved more simply as at the inclined part. The glass panes were directly mounted to the basic frames sealed with graphite and pressed by steel frames with bolted assembling. The cross-section of these channels stayed unchanged at 50 x 250 mm². In addition 6 impulse pipes for pressure measurement were integrated in the horizontal channel. All measurement positions are located at the top of the horizontal channels and distributed almost equal along it.

At the left side of Fig. 2 the RPV simulator is arranged. This tank serves as a model of the reactor pressure vessel. It feeds the hot leg with gas and receives water flow from the channel. The top part of the tank is equipped with a standard perforated plate, to allow an almost uniform gas distribution. The dimensions of the tank are similar to the SG separator (0.6 x 0.8 x 1.6 m³).

The test section parts and both tanks are connected among each other by rectangular flanges with graphite seals and bolts. All connections, inner areas and details were designed and manufactured in consideration of high quality standards, small deviations and tolerances, to avoid unneeded flow disturbances. Information about the detail design with all measures (as built) is attached to this report as App. 1. The CCFL test rig was erected at a moveable platform. While the SG separator was fixed permanently, the test section and the RPV simulator were mounted to be movable, in order to compensate the thermal elongation during operation.

2.2 Thermal insulation concept

In agreement with the work packages of the TOPFLOW project CCFL tests were scheduled for air-water- and steam-water flows. Hence the test rig works under high temperature condition and an effective thermal insulation concept had to be developed. The surface area of the test rig may be divided in 2 parts: On the one hand there are metal sheets and pipes otherwise the observation possibility requires transparent windows for picture recording and illumination.

The first type of non-transparent areas is insulated by covering it with plates or blankets of pure inorganic and open porous material. The investigation of different insulation materials already was done during the TOPFLOW-II project (project number 150-1329) and described in detail in [1]. As result of this task 2 types of thermal insulation were found. Both have almost the same compounding that includes metal oxide fibers. Planar areas are covered with plates of Multitherm 550 with a thickness of 30 mm. The relative high density of 130 kg/m³ results in a fine porous structure and provides finally a good insulation capability under high pressure. Usually the metal plates are covered with 2 layers of Multitherm in such a way that the gaps are not super-imposed. Finally, stainless steel sheet are used to protect the insulation from humidity and mechanical damage (Fig. 4).

Fig. 4   RPV simulator, insulated with Multitherm

Fig. 5   Water outlet pipe with Superwool wrapped insulation

For insulation of curved areas (pipes, flanges) a similar material is used, but it is manufactured as blanket (Superwool SW 607 blanket 128) with a density of 128 kg/m³. Before it can be used, the blanket is cut in strips of about 10 cm width. Due to it thickness of 13 mm the strips can be wrapped helically around the pipes. To avoid gas diffusion through these insulation packings, between each layer a very thin stainless steel foil (50 µm) is added. Normally complete pipe insulation consists of 4 – 6 layers and is finished by a steel foil as protection (Fig. 5).

Of course both insulation techniques allow pressure equalization to endure pressure changing of the ambient gas atmosphere.

Observation windows are the second kind of surface areas at the test rig. It is obviously that the insulation method described above is not usable. So 2 other techniques were developed and applied at the TOPFLOW facility: The first bases upon thermal stratification. The observation object is enveloped with a thermal insulated steel cap that is opened at the bottom side. If the observation object is heated-up, due to heat losses the gas temperature around it is increased and it density decreases. So the hot gas remains under the cap and the observation object is thermal insulated. The optical observation is possible from the bottom side using mirror systems.

A second and smarter method is the application of thermal insulated glass windows. Thereby a package of glass windows is assembled in such a way, that some identical glass panes are put on each other. Between the panes PTFE tape is laid at the circumference. So closed gas volumes form that serve as thermal insulation. During assembling it is important to hole the PTFE tape at bottom position of the glass package, to allow pressure equalization. This technique was applied the first time at TOPFLOW on the DENISE test basin to insulate the LED illumination modules against the hot fluid inside. During DENISE measurements the functionality was proven. Hence this method is used on the CCFL test section to insulate the big glass windows at the SG inlet chamber module and at both horizontal modules. Fig. 6 shows the first one with complete insulation. Here a package of 4 glass panes is applied that is mounted directly to the inner temperature proof glass window and assembled by steel outriggers. The PTFE

Fig. 6   Thermal insulation of the SG inlet chamber module

strips are well visible at the vertical and bottom horizontal part of the circumference. Around the glass package the thermal insulation is made from Multitherm 550 with a final steel protection layer. At the left side in the middle part of Fig. 6 two thermocouples are shown. They were used to monitor the temperature in the inner gap and at the outer side of the glass package. While the inner temperature proof glass pane has a thickness of 15 mm, the glass panes of the package are thinner (5 mm). The last one has dimensions of 897 x 882 mm². Both types were made from Borofloat 33 glass, manufactured by the German company Schott. Further information contains the data sheet in App. 2. The glass packages of the horizontal test section modules are prepared in a similar way. These 4 panes have a size of 903 x 270 mm². Of course both sides of the transparent modules are equipped with insulated glass windows to allow the flow illumination.
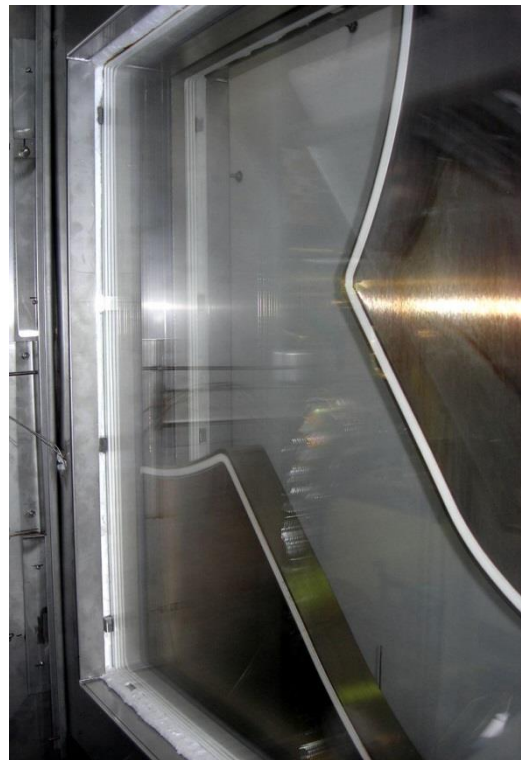
2.3 TOPFLOW pressure tank

The CCFL tests were scheduled not only for cold air-water but also for hot steam-water condition. To allow a steam – saturated water equilibrium the pressure around the test rig have to correspond to the saturation pressure as function of the steam temperature. For this reason the complete CCFL test rig is operated in the TOPFLOW pressure tank. This tank has an inner diameter of 2.44 m and an inner length of 7.24 m. It is equipped with a big lid that allows an access to the tank over the complete inner diameter. The maximum operating pressure is 50 bar and the inner temperature may increase up to 70 °C without inner electronical devices. Otherwise 50 °C should not be exceeded. The tank can be pressurized with pure air by a compressor station or with nitrogen by a high pressure nitrogen supply unit. Both auxiliary systems require about 5 h for a complete tank feeding. Despite an effective thermal insulation heat losses from the test rig lead to a heat-up of the tank atmosphere. To allow normal working condition, especially for electronical devices, the tank is equipped with a gas/air cooling system that works under the operation pressure. The maximum cooling power achieves 30 kW according to the temperature difference between the tank volume and the ambient air. Fig. 7 shows a simplified scheme of the pressure tank including the significant peripheral auxiliary systems.
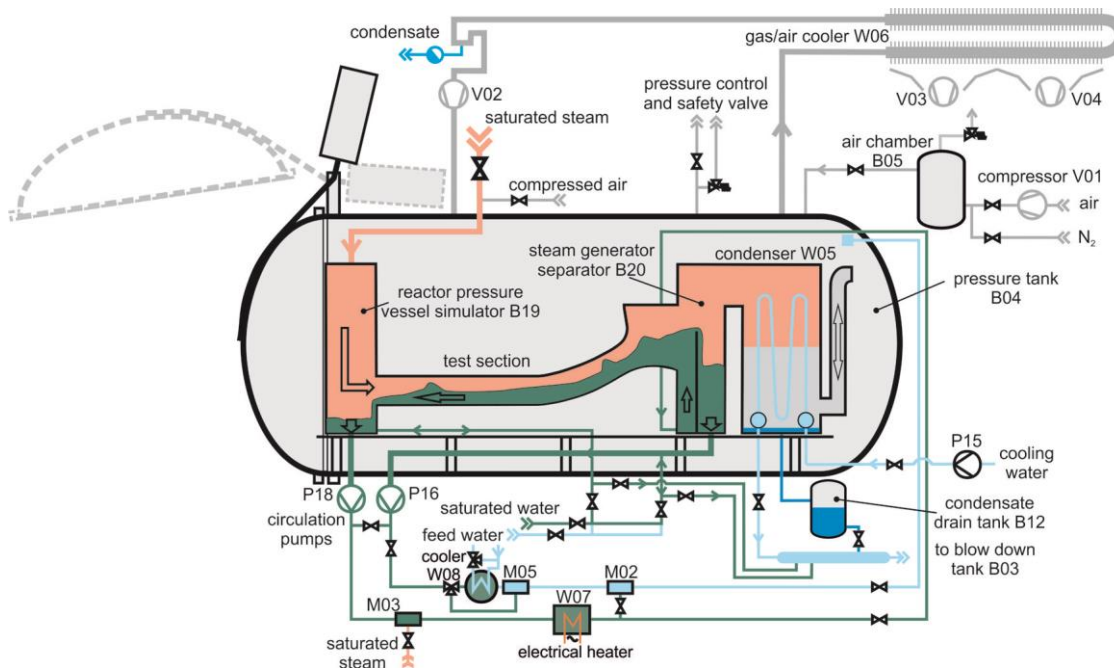
Fig. 7   TOPFLOW pressure tank with installed CCFL test rig (simplified)

The working principle of the pressure tank is based on pressure equilibrium between the tank atmosphere and the inner volume of the test sections. Thanks this technology the test rigs don't have to resist the compressive forces and may be assembled with thin walls and big observation windows. A major role for the pressure equilibrium technology plays a high pressure condenser that separates the steam inside the test section from the gas tank atmosphere. While steam flows into it from the upper side the bottom part is opened to the tank atmosphere. Due to the density difference between steam and gas a stabile stratification appears (Fig. 7) whereat the level of the separation layer depends on the received steam mass flow respectively the condensation power.

An important improvement to the previous facility configuration was the completion of the pressure tank with two circulation loops that are shown at the bottom part of Fig.

7. Both loops contain pumps which circulate the liquid through the test rig. One loop serves to heat-up the water, if necessary near to saturation level, by a mixing steam heater (M03) and additional an electrical heater (W07) for the fine temperature regulation. The second one works as cooling loop. It is equipped with a heat exchanger that is cooled by the TOPFLOW auxiliary system. To allow a wide range power operation two bypasses are available: one for the cooling water and the other for the high pressure fluid. Both loops are connected together as directly at the pressure side of the pumps as downstream the heating / cooling devices. So a high flexibility of the media supply is possible.

Fig. 7 illustrates the pressure tank prepared for CCFL operation. In this case the suction-side of the pumps was connected to the bottom outlet pipe of the tanks B19 (RPV simulator) and B20B (SG separator) respectively. As visible at Fig. 7 the cooling loop is closed by a blind flange, because it is not necessary for these tests. Here the pipe connection between the pressure sides of the pumps was permanently opened to pump water from both tanks through the heating loop into the tank B20A.

The piping directly below the pressure tank serves for filling and draining procedures of the test rig. Below the condenser a condensate drain tank was installed that improve the condensate drain from the condenser significantly and allow a minimum condensate level in it. This is important for a reliable operation of the high pressure condenser in relation to a free gas exchange with the tank atmosphere. Furthermore the pressure tank is equipped with a pressure controlling system and a safety valve.

2.4 Operational measurement technique and calibration procedures

The TOPFLOW test facility was designed as research facility. Hence also the pressure tank is well equipped with measurement technique. It includes temperature, pressure, mass- and volume flow, electrical parameters as well as gas concentration sensors. On the TOPFLOW facility a special code system is used to mark each device definitely. The sensor label consists of 2 – 4 letters, followed by a numeral and a number. The 1st letter marks the sensor type: T – temperature, P – pressure, PD – differential pressure, L – level, E – electrical parameter (voltage, current, power), F – mass- or volume flow, Q – concentration or thermal power. The next letter is I for indication. Then may follow: C for controlling, S for switch, Z for limitation and A for alarm. The 1st number marks the relating system: 1 – steam generator, 4 – test section circuitry and 8 – pressure tank and peripheral systems. After the hyphen a unique number for each sensor completes the label. The valves are marked in a similar way: first a unique number for each device and then a letter string consists of 3 letters: A – isolating or R – controlling; V – valve or H – ball valve; A – with power unit or H – manual operation.

The TOPFLOW process controlling system allows a remote control of the facility operation as far as possible. Like already described in [1], most sensors scale a measured physical value and transform it to a standard output signal (0-10 V or 4-20 mA). These sensors are connected to electronic devices that convert it signals into digital information. The electronic devices are combined in groups and connected to Interbus modules, which manage the communication among each other and with an OPC server. This server stores the data and delivers information for visualization and controlling. Additionally, it serves as data source for the operational data logging system.

Fig. 8 illustrates the location of each measurement sensor on the CCFL test rig and at the peripheral systems of the pressure tank, the air supply unit and the steam generator. Design and function of the 1st and 2nd one were already explained above. The air supply unit consists of 6 parallel legs that combine a volume flow sensor, a control valve and an isolating three-way cook each. 6 legs are necessary to allow high gas supply accuracy. The CCFL tests require the operation of the largest 2 legs: FIC4-10 and FIC4-11. The steam for the hot tests was produced in the steam generator circuitry (Fig. 8 left side). The primary device of it is an electrical steam generator that may produce maximal 1.4 kg/s saturated steam with 4 MW energy consumption. It was designed as once-through forced-flow boiler, whereat a powerful centrifugal pump allows the water circulation. A vertical tank separates the two-phase flow from the steam generator outlet. The liquid phase from the separator is returned into the steam generator after slight sub-cooling. The last is necessary to avoid cavitation at the suction side of the circulation pump and to control the steam pressure. The steam from the separator tank on the one hand flowed to the test section and on the other hand was used as heating steam in the mixed heat exchanger M03 if necessary. The removed steam mass flow was replaced with cold feed water.
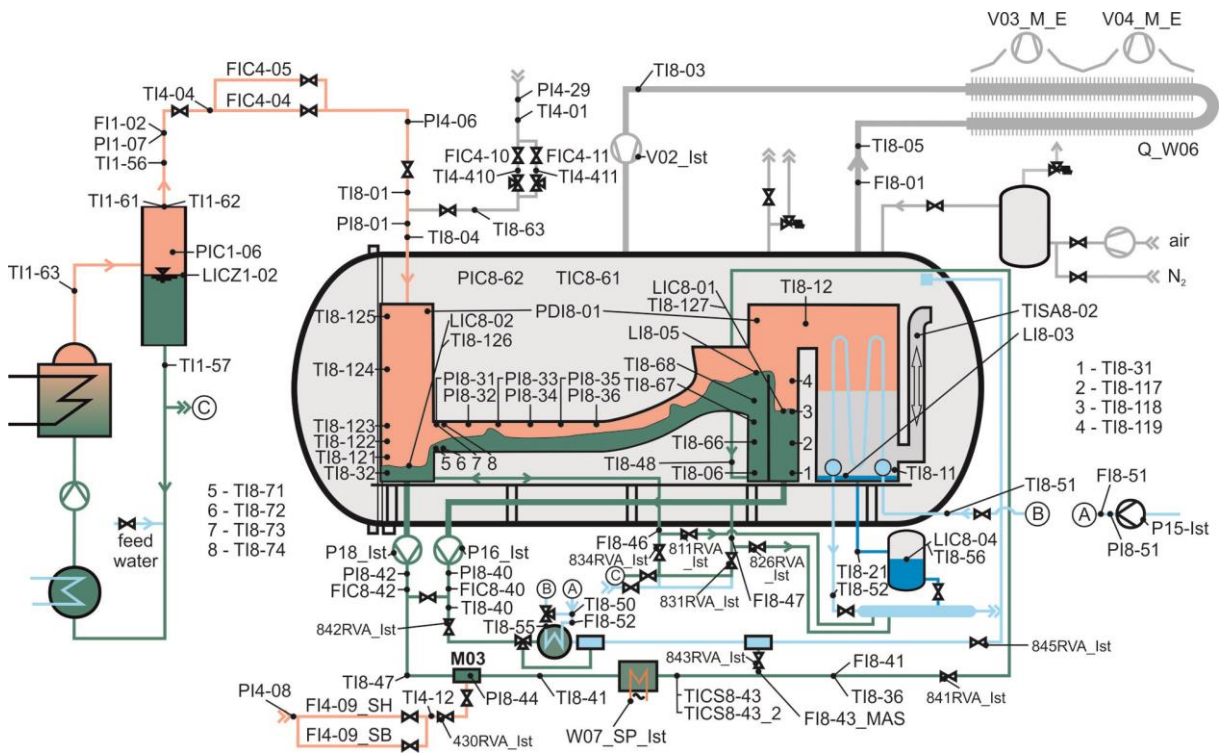
Fig. 8   Arrangement of the operational measurement technique on the CCFL test rig

The scheme above includes almost all sensors and valves for which data were recorded during the CCFL tests by the operational data logging system with a frequency of 1 Hz. The data logging at TOPFLOW is realized with DIAdem software developed by National Instruments. DIAdem stores the data files in its own format and so after completion of the measurements, all data were converted to MS Excel. The Excel sheets are grouped according to the test parameter. Attention is invited to the fact that there are slightly differences in the Excel data for air-water- and steam-water tests, because partial different sensors and devices were applied. For clearness a register of all stored data is attached to this report as App. 4. Beside the

sensor code, it contains the dimension, a parameter description, the sensor type, the calibration range, the calibration date, information about the maximal residual deviation and some comments. At the end of this register some digital parameter are added for the sake of completeness.

While temperature, pressure or flow parameters are measured directly, the level in the tanks has to be determined indirectly. For it the differential pressure is measured between a connector at the top of the tank with gas atmosphere and a bottom point of the tank with connection to water inventory. Thereby the impulse pipe between the differential pressure transmitter and the upper point is filled with water to a fixed level. So the transmitter measures the difference between the full impulse pipe and the water level in the tank. The latter is calculated in accordance to:

$$L_L = \frac{L_{imp} * (\rho_{imp} - \rho_G) - \frac{\Delta p}{g}}{(\rho_L - \rho_G)} \tag{1}$$

Here L_L is the water level in the tank, L_{imp} – the distance between the lower and upper connection point of the impulse pipes, ρ_{imp}, ρ_G and ρ_L – the densities in the impulse pipe, of the gas and water in the tank respectively. Δp is the differential pressure and g the gravitational acceleration. Regarding to Fig. 8 all levels on the CCFL test rig:

- RPV simulator (B19) LIC8-02,
- SG separator tank A (B20A) LI8-05,
- SG separator tank B (B20B) LIC8-01,
- Condenser W05 (LI8-03) and
- Condensate drain tank (LIC8-04)

are calculated continuously by the TOPFLOW process control system (PCS). Thereby the densities are determined also by the PCS using an approximation to the thermal hydraulic properties of water, steam and air IAPWS-IF97. In the operational range of the TOPFLOW facility the thermal hydraulic property approximations have an uncertainty less than 1%. The gas density is chosen as function of the gas temperature: If it is less than 10 K below the saturation temperature (t_s) then the gas density is equal to the air density. If it is ≥ t_s, then the steam density is valid. In the transient region a linear interpolation is used. For an accurate calculation of the tank water density some thermocouples, distributed over the tank height (Fig. 8), are used. In accordance to the level in the tank, all temperatures below it are averaged. To avoid undesired temperature fluctuation a hysteresis of level limits are considered. Additionally, the water temperature in the impulse pipe is measured and used for density calculation. While the level in the B19 tank (RPV simulator) is calculated with the pressure PI8-01, for the other 4 tanks (B20A and B, condenser and condensate drain tank) PIC8-62 is used. Despite the high accuracy of the PCS defined level values, all information for a later level calculation is additionally included in the Excel sheets. Similar to the tank levels the cooling capacity of the gas/air cooler (Q_W06) is calculated by the PCS. For this the gas heat capacity as function of temperature and pressure is approximated and multiplied by the gas mass flow (as a function of density and volume flow) and by the inlet – outlet temperature difference of the cooler W06.

Additionally to the previous hot leg tests 6 pressure sensors were installed at the horizontal test section modules, to get information about slug behavior. Their measurement positions were defined at the upper end of the horizontal channel and almost equally distributed over the channel length. The correct position may be

looked up at the technical drawings in App. 1. Furthermore 4 thermocouples are available: 2 at the upper end and 2 at the lower end of the horizontal channel near the flange connection to the RPV simulator.

To provide test data with high accuracy, the relevant measurement channels have to calibrate periodically. For this purpose the sensor is connected to a reference device and a characteristic over the calibration range is recorded. It compares the reference value with the indication of the PCS, so it is ensured that not only the sensor but also the electronic devices (e.g. analog digital converter, Interbus modules and cold end compensation) are considered. The thermocouples and resistance thermometer are examined by a metal block calibrator (type Beamex FB350), that is periodically checked by a certified laboratory. In case of deviation to the reference value, a correction polynomial is added to the lower data processing level of the PCS.

The calibration of pressure and differential pressure sensors are done by parallel connection of it and a reference device to a pressure source (calibration hand pump). As reference in this case an UNOMAT MCX/1910 is applied. Then by the pump a characteristic line is adjusted and both pressure indications are recorded. If deviation occurs, a sensor-internal routine is used to compensate it. After changing of the pressure sensor configuration the comparison with the reference device is repeated until satisfied results are achieved.

Furthermore a lot of flow measurements with different sensor types are used. The air volume flow to the test section is quantified with thermal mass flow meters manufactured by the company Bronkhorst (type IN-Flow). While the largest channel (FIC4-10) is assembled with separate flow sensor and control valve, the FIC4-11 is a combined device. Due to the measurement principle well-designed inlet flow condition are necessary. To allow a low measurement uncertainty, all necessary flow meters are calibrated usually by the manufacturer Bronkhorst before new air flow tests are scheduled. Beside air flows, steam mass flows are defined by ISA or Venturi nozzles in combination with Rosemount 3095MV transmitters. This principle was chosen because it is less sensitive to condensate drops flowed through the nozzle. It works by measurement of the pressure drop over the nozzle and determination of the volume flow using geometrical and thermal hydraulic parameters. Then the mass flow is calculated with the steam density approximated in the 3095MV. The necessary accuracy requires 2 measurement channels for each flow parameter due to the wide pressure operation range of TOPFLOW. Thanks to very low erosion of the measuring section, a periodic calibration is not necessary and the calibration information of the manufacture is used.

The water mass flow is measured by Coriolis flow meters (FIC8-40, FI8-41, FIC8-42, FI8-46, FI8-47 and FI8-52) and with Vortex flow meter for FI8-43 and FI8-51. The Vortex devices use sensitive pressure sensors to detect vortexes after a well-defined obstacle in consideration of the Karman vortex street. Both devices don't consider a variable operating temperature. The FI8-51 measures the cooling water flow that is almost constant at about 30 °C. This temperature is configured in the device and hence the measured value is valid. In opposite, the fluid temperature in the FI8-43 may change in a range of 20 – 264°C. So the output value is corrected in the PCS according to density ratio. Also for these flow meters the manufacturing calibration is used, whereat the Coriolis meters were obtained only some years ago.

The maximum residual deviation of the calibrated devices is available in App. 4. Further information about the applied measurement technique contains [1].

2.5 Inspection of the air flow meters FIC4-10 and FIC4-11

As aforementioned the air volume flow meters uses a thermal measurement principle. It requires a well-defined gas flow through the sensor that needs a sufficient inlet length upstream the sensor. During the previous hot leg tests, problems with the accuracy of FIC4-10 appeared. A post-measurement examination of the sensor assembling revealed an incorrect diameter of the mounting flanges and an insufficient inlet length. So the air volume flow had to be corrected as reported in [1]. Furthermore the diameter of the in- and outlet pipe was increased up to the correct values and the inlet length was extended to 15D that is more than the manufacture recommendations.

Bearing in mind these troubles, calibration tests with the FIC4-10 and FIC4-11 sensors were conducted before the current CCFL air-water tests was started. As reference device a high volume flow rotameter (Yokogawa type RAMC08, see Fig. 9) was used. Beside the rotameter indication the pressure drop over it, the air outlet temperature and the ambient pressure at sea level were recorded to covert the rotameter volume flow to standard condition. This procedure was done in consideration with equation 3.2 and 3.3 in [1]. In comparison to the previous deviation of about 22 %, it decreases to a range between 1 % (500 nm³/h) and 11 % (1000 nm³/h) for the 2015 comparative measurements.

Nevertheless these uncertainties are significant higher than the residual deviation after manufacture calibration from 2015 (-0.4 – 0.7 % of measurement value FIC4-10), whereat the reason is unknown. To avoid useless measurement data, correction polynomials were calculated and added to the lower data processing level of the PCS. Of course, the changed measurement channel was checked with new comparative tests resulted in a residual deviation of ± 0.15 %. This value is significant lower than the uncertainty of the rotameter and so the FIC4-10 was applied for the scheduled CCFL tests. The deviation between the FIC4-11 and the rotameter was found in a range between 0.5 and 3 % that is acceptable in consideration of the residual deviation after manufacture calibration (-1 – 1.5 %) and the rotameter uncertainty. Hence this measurement channel was not corrected.

Fig. 9 Comparative tests with the flow sensor FIC4-10

A few months later after completion of the tests the FIC4-10 and FIC4-11 sensors were re-examined. This time the deviation was found between 1 and 1.6 % for FIC4-10 as well as -0.4 and 4.4 % for the FIC4-11 respectively. During data analysis these uncertainties were considered by correction functions in the Excel sheets.

3. Special measurement technique

3.1 Visual observation

A further important task of the CCFL project was the observation of the flow structure along the complete horizontal channel and inside the inclined test section module. Thereby for the first one two cameras of the type SYGONIX 43176S were applied. They may provide pictures with maximal 1600 x 1200 pixels and a resolution of 2 mega pixels CMOS. To observe the entire length of the channel without a mirror system each camera was equipped with a wide-angle lens (O-FB/2.8) with a fixed aperture. To avoid the wide-angle picture distortion as much as possible, the middle plane of the lens was adjusted to the bottom edge of the horizontal channel. So the interesting image section, a long small stripe, may be recorded in an acceptable quality. During the CCFL tests picture sequences were recorded with a frequency of 60 Hz and an image size of 1280 x 720 pixels.

As the previous tests revealed, the flow behavior in the inclined module is more turbulent and has to be observed with a higher frequency. So a high speed camera of the type AOS Q-VIT was used for this purpose. This device works with a progressive CMOS (8 μm pixel size) with maximal 1696 x 1710 pixels. It is very light sensitive up to ISO 3200 on monochrome modus. The camera achieves a maximum frame rate of 100000 fps, however at a very low image size. During the current tests the CCFL high speed picture sequences were recorded with an image size of 1250 x 1250 pixels and a frame rate of 500 fps for 13 s, so that 6500 single images used the available camera memory of 10 GByte to full capacity.

The cameras were installed inside the TOPFLOW pressure tank. As afore-mentioned commercial non pressure-proof devices were applied. So it had to be protected from damage by

Fig. 10 Installed CCFL test rig with 3 camera containers in the right position

installation in pressure-proof boxes. These one are designed as cylindrical one-side closed containers with an observation window at the front side that may be opened for installation and service purposes. During operation the cameras release heat that is removed from the containers to the ambience by air flushing. Fig. 10 shows both web-cam containers in the foreground and the high-speed camera box behind it.

The communication between the cameras and the control-PC was organized via Gbit LAN. The picture sequences of all 3 cameras were synchronized with the operational data by a trigger signal. Thanks a trigger input on the high-speed camera, it can be activated directly. Because the web-cams don't have this possibility, a LED was placed in the captured image sector of each camera that glowed over the
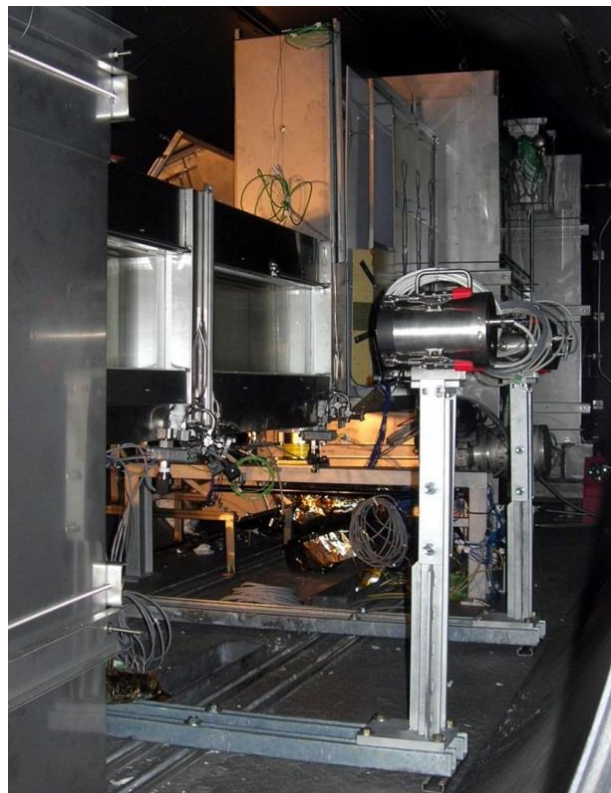
25

measurement time [1]. Additional the trigger signal is stored in the operational data files as last digital data channel (START3), see App. 4. The activated trigger is indicated by a non-zero value.

The interesting observation sector of the inclined test section module is a sizeable area. So, during the test section design the optical path was analyzed in consideration with the optical properties of the high-speed camera lens and the available space. This results in a quite long distance between the object and the camera position that was only practicable in the pressure tank with a double mirror system. Fig. 11 illustrates the position of the camera container, both mirrors and the test section module. All components are moveable mounted in supporting frames, so that a fine alignment of the image position and size was possible during commissioning.

Fig. 11 Sectional view of the test section module, the optical mirror arrangement and the camera container

3.2 Illumination

It is obvious, that an optical observation of the flow structure inside a closed pressure tank is only possible with a powerful illumination. During the previous hot leg experiments first tests with LED illumination were conducted.
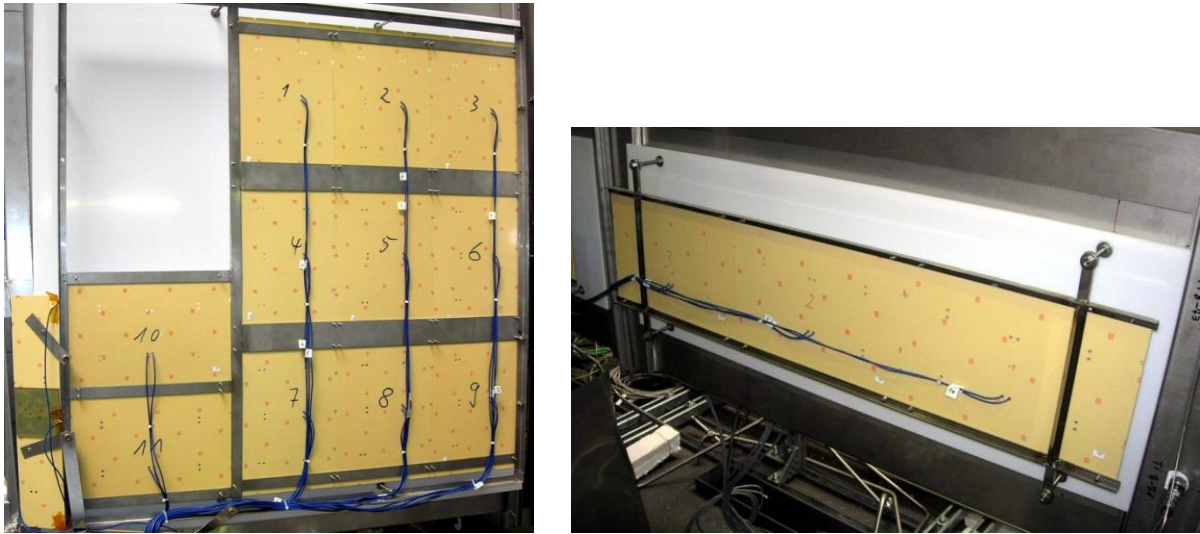
Fig. 12 Illumination of the SG inlet chamber module (left) and the horizontal test section module (right)

Unfortunately it was impossible to guide the light to the object of interest under the thermal insulation cap (steam-water tests) in a homogeneous way, because no

parabolic mirror could be manufactured in the necessary quality. So, that kind of LED illumination was applied only for cold air-water experiments, where a direct illumination of the inclined test section module was possible. The light quality in the last case was good and the light was homogeneous distributed. After this illumination tests a fiber optic system was tried [1] for steam-water experiments. It was powered by a gas-discharge lamp and the light was guided through fiber optic bundles under the insulation cap, where some single wide angle modules distributed it. Despite the application of a diffuser plate between light sources and test section, at the captured images the illumination was insufficient because hot spots appeared.

Keep these results in mind, only a LED illumination with a lot of single light points is considered. Thanks to improvement of the LED technique new passive cooled LED panels of the type BacklightMatrix V2 manufactured by LUMITRONIX (App. 3) could be used. The new thermal insulation concept results in a much better access to the object of interest, so that the LED panels now are equally distributed parallel to the glass windows. Despite the narrow arrangement of the single LED at the panel a diffuser plate is installed between the panels and the glass panes to further homogenize the light flow. Fig. 12 (left picture) shows 12 LED panels with 70 single LED's each, assembled to a holding frame at the SG inlet chamber module. Furthermore the diffuser plate is visible. While the distance between the panels and the plate was determined as 50 mm, the diffuser plate is about 100 mm away from the outer insulation glass pane. This configuration was found as an optimum for a homogeneous illumination. The smaller windows at the horizontal test section modules were illuminated in a similar way (Fig. 12, right picture). Here twice 3 panels with also 70 single LED's are applied.

All panels are connected to power transformers (type: SIEMENS SITOP power flexi 6EP1 353-2BA00) that are controlled by the TOPFLOW process controlling system. So the illumination power is controllable and can be adapted to the flow condition and to the camera requirements.

3.3 Additional pressure measurement

The results of the previous hot leg tests reveal that it is important to investigate slug frequencies according to the test parameters. To do so, parallel to the optical observation pressure signals along the horizontal part of the test section should be recorded. Unfortunately the number of pressure-proof pipe-ducts through the tank wall is limited that leaded to the decision to install the sensors inside the tank. So 6 sensors (type: BD SENORS DMP 331) were checked under pressure tank conditions with positive results.

As the best location for the measurement of dynamic pressure signals the upper part of the horizontal channel was found. Hence, already during the test rig design 6 fittings were almost equally distributed over the channel length. The first one is located near the connecting flange to the RPV simulator and the last – near the inclined test section module. The fittings were connected to the below arranged pressure sensors by impulse pipes. This configuration allows a constant hydrostatic head above the sensors independent of steam condensation in the test section.

As reported above, the TOPFLOW data acquisition system stores the parameter with a frequency of 1 Hz. In accordance with the data evaluation results of the previous

hot leg tests a faster data logger for the pressure sensors was obtained. The device (BD SIMEX PAC-99X) stores maximal 48 analog data input channels with a frequency of 10 Hz. It provides the data files in *.csv format, so that it is available in common MS Excel. Similar to the high-speed camera also the data logger is synchronized by a TTL trigger signal generated by a special electronic device, called trigger box.

Despite the preliminary checking of the pressure sensors, first problems appeared already during the CCFL tests. Nevertheless the pressure data were recorded until the end of the test series. A final inspection after completion of the measurements resulted in malfunction of all pressure sensors installed inside the tank, expect two sensors on the horizontal test section module (PI8-31 and PI8-33). Probably the periodical pressure changing inside the tank led to the sensor damage.

4. Experimental procedure

4.1 Test matrix

After completion of the test rig erection, the installation of the measurement technique and the connection to the TOPFLOW facility further preparing tasks were necessary before the real tests could begin. First of all, it is important to define the thermal hydraulic boundary condition for the measurements. Based on the old hot leg test results it was decided that in the frame of the current project only CCFL tests were conducted. Bearing in mind that the design of the SG simulator was significantly changed, the knowledge of the previous CCFL tests couldn't be used for the planning of the current experiments. Especially the gas volume flow for the onset of flooding and the zero penetration point (complete CCFL) had to be redefined. Therefore, after definition of the injected water mass flows, pretests with air and water at ambient pressure were carried out to detect the new gas flow limits. This information was used to prepare the test matrix for cold air-water flows. Then these tests were completed and the results were used to calculate the new flooding characteristic in terms of Wallis parameter. On this basis the CCFL steam mass flows were defined in consideration of the pressure levels that led to the thermal hydraulic parameters for the steam-water matrix. Finally a second air-water series was scheduled to investigate the flooding characteristic for a doubled pressure level of 2 bar.

Tab. 1: Test matrix for the air-water CCFL tests

Pressure [bar]	1						2			
Water mass flow [kg/s]	2		1		0.3		2		1	
Test number / Gas volume flow [m³/h] norm			11	432.8					230	574.7
			12	442.0					231	625.7
	1	484.2	13	471.8	23	483.5			232	706.6
	2	508.5	14	506.7	24	506.6	210	808.2	233	757.6
	3	608.3	15	608.3	25	607.5	211	879.3	234	828.3
	4	556.8	16	557.5	26	557.1	212	777.8	235	737.8
	5	506.3	17	506.4	27	506.5	213	717.3	236	686.5
	6	458.9	18	459.2	28	488.3	214	656.0	237a	635.5
	7	414.4	19	414.4	29	476.0	215	574.5	237b	635.6
	8	313.5	20	366.2	30	467.5	216	498.4	238	584.6
	9	258.6	21	356.1			217	458.0	239	544.0
	10	246.8	22	345.7			218	413.6	240	513.6
							219	364.8	241	492.1

Tab. 1 and Tab. 2 show all CCFL tests, conducted in 2015. The experiments are arranged according to pressure and water mass flow. The columns include pairs of unique test numbers and associated gas volume flow rates. Each column groups the single tests of one series, starting with a counter-current flow (green colored), as next tests with increasing gas flow (CCFL) up to zero penetration (blue labeled) and further with decreasing gas flow down to the collapse of CCFL. Finally a counter-current flow test (green) was completed the series. Some tests were repeated for reproducibility (e.g. 46b and 47b).

Tab. 2 Test matrix for the steam-water CCFL tests

Pressure [bar]	10						25						50			
Water mass flow [kg/s]	2		1		0.3		2		1		0.3		2		1	
									120	535					180	683
			60	297	80	346			121	577					181	738
			61	355	81	384	100	580	122	636	140	553	160	687	182	801
	40	329	62	391	82	420	101	672	123	692	141	626	161	879	183	848
	41	447	63	448	83	479	102	741	124	764	142	806	162	1050	184	967
	42	410	64	411	84	393	103	615	125	664	143	603	163	838	185	889
	43	373	65	377	85	372	104	545	126	603	144	586	164	772	186	823
	44	333	66	326	86	349	105	492	127	533	145	570	165	704	187	760
	45	294	67	280			106	430	128	491			166	635	188	698
	46a	254					107	372	129	469			167	574	189	658
	46b	257					108	323	130	417			168	514	190	608
	47a	217											169	477		
	47b	212											170	417		

(Left axis label: Test number / Steam mass flow [g/s])

The gas flows in both matrixes are corrected values. So, the norm air flow was adjusted in consideration of the results of the post measurement re-examination of the air flow meters FIC4-11 and FIC4-10, see section 2.5 Inspection of the air flow meters FIC4-10 and FIC4-11. The steam mass flow was corrected in accordance to the heat losses in the steam pipe and to the results of energy- and mass balances in the test rig – condenser unit (see section 6.2.2 Steam-water flow).

Already a first view at the matrixes reveals that the CCFL phenomenon is non-symmetrically related to the zero penetration point. It means, that the CCFL starts significantly later during increasing gas flow and it stays longer in the case of decreasing gas flow. Already the pretests showed a second effect: for all series with 1 kg/s injected water mass flow the CCFL starts significantly earlier than for comparable series with more (2 kg/s) or less (0.3 kg/s) water flows.

4.2 Facility preparation and test procedure

After definition of the thermal hydraulic boundary condition and the test matrixes now the preparation of the TOPFLOW facility will be explained. First of all the operational sensors were checked and the impulse pipes were flushed to allow a proper operation of the level measurement in the tanks and the pressure sensors. Then the observation technique, the mirror system and the illumination were finally tuned. Additionally at the beginning of each measurement day the following operations were done:

- the measurement PCs were switched on,
- the high-speed camera, the web cams and the data logger of the special pressure sensors (section 3.3 Additional pressure measurement) were powered on,
- the air flushing system for camera container cooling was activated,
- the remote control of the cameras and the special pressure sensors from the control room was established,
- the acquisition of the operational parameters was activated,
- the trigger system was checked and

- the LED illumination was switched on.

The further facility preparation depends on the test type. The CCFL measurements started with air-water tests at ambient pressure condition. For this the TOPFLOW pressure tank was opened, so that the air flow could be discharged to atmosphere. The slight overpressure in the test rig due to the pressure drop of the flowing air was considered in the data evaluation. Then water was injected into the tank B20A (SG simulator, see Fig. 2), its level increased and the water flowed through the test section into the RPV simulator B19. On the TOPFLOW facility the experimental circuitries are filled with demineralized water with an electrical conductivity of about 1 µSm/cm, but less than 5 µSm/cm. It allows a safe operation of the facility without stress corrosion. The filling procedure was continued and the level in the test rig increased over the steel sheet in the SG separator, so that the water flowed in the B20B tank. The water injection was stopped when the water level in B20B tank reached about the half height of the steel sheet. Then the pumps P16 and P18 were switched on to circulate water from both tanks (B19 and B20B) into the B20A and further as through the test section in the B19 as over the steel sheet in the B20B tank. The valves were adjusted respectively. This operation was continued until both circulation loops were free of air inclusions. After this the level in the RPV simulator was decreased to a height that allows a free water discharge from the horizontal part of the test rig into the B19 (about 0.3 m). To avoid a decrease of the B20B level the pump P16 was switched off, because due to the level decrease in the test section no more water flowed over the steel sheet in the B20B tank. Now the air flow was activated by the controller FIC4-11 / FIC4-10 and increased up to a value that allowed a counter current flow near the limitation, but without CCFL. Parallel to this action the injected water mass flow was adjusted to the nominal value.

Then during a minimal period of 10 minutes the operational parameters were kept constant and after this time span the measurement was started by activating of the image recording of both web cams. After this the high-speed camera, both indicator LEDs for the web-cams and the data logger of the special pressure sensors were triggered. Thereby the high-speed camera captured images for 13 s, the web cam LEDs glowed for 60 s and the pressure signal was recorded with the 10 Hz frequency also for 60 s. Only for the first 3 air-water tests at 1 bar the capturing time for web cams and pressure sensors was 30 s. After completion of the triggering the web cams were switched of, the air volume flow was increased up to the next matrix point and the measurement procedure starts again. Due to the increasing gas flow the CCFL started and the water flow from the SG separator to the RPV simulator was obstructed (onset of flooding). This effect led to water retention in the tank B20A and hence to a level increase and finally to a water flow over the steel sheet in the B20B tank. To control the water balance in the B19 and B20B tanks the pumps P16 and P18 were used together. The pump flow rates were adjusted in accordance with the obstruction level of the CCFL. The flow condition is schematically illustrated at Fig. 7.

As Fig. 13 shows, the achievement of the zero penetration point was checked by the observation of the water level in the horizontal channel. During complete CCFL the channel part near the RPV simulator was free of water (red oval). After zero penetration point test the gas flow was decreased stepwise and further CCFL data was recorded during deflooding. The last test of a series with constant pressure and water mass flow was a counter-current flow experiment slightly below the CCFL collapse.
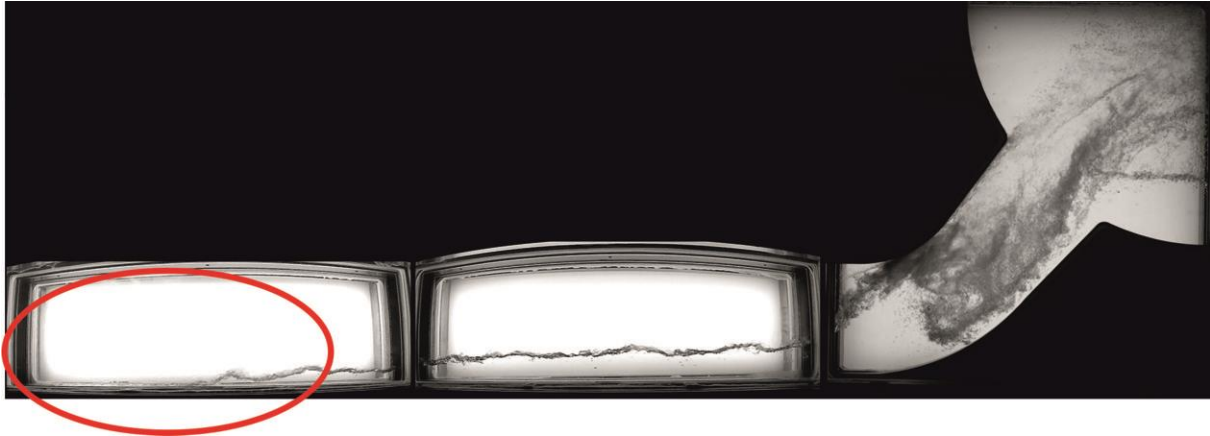
31

Fig. 13 Photo composition of synchronous images of all 3 cameras, matrix point 162: 50 bar steam-water test with 2 kg/s injected water- and 1.05 kg/s steam mass flow, zero penetration condition

After completion of the 2 kg/s water injection test series this parameter was decreased to 1 kg/s and 0.3 kg/s. Each time a test series similar to the aforementioned procedure was executed.

In principle all three air-water test series at a pressure of 2 bar went on in a similar way. Of course the TOPFLOW pressure tank was closed and the injected gas flow was used not only to generate the flow structure but also to increase the pressure in the tank. So, beside the water mass flows, the tank levels and the gas flow, the pressure had to be controlled. Due to a very low nominal pressure it was adjusted manually. During the air-water tests the fluid temperatures were observed but not controlled, because the air temperature can't be influenced on the TOPFLOW air supply system and the changing of the liquid temperature during the measurement was in an acceptable range. Both temperatures respectively its gradients were considered during data evaluation.

The next step was the preparation of the facility for steam experiments. For this purpose, parallel to the activities on the pressure tank, the steam generator was put into operation. Since this part of the facility is an auxiliary system, its operational procedures are of minor relevance and not described in this section. Before steam operation could be started, the test rig was filled completely so that the glass windows were covered with water. Then, during circulation pump operation (P16 and P18) the entire test rig and the circulation loops were heated-up continuously by the electrical heater W07. If a pressure increase was scheduled, both activities were done together, whereat the pressure rise was done by the TOPFLOW nitrogen supply unit. The maximum power of the W07 (30 kW) allows a smooth preheating up to app. 80 °C with an acceptable temperature gradient of about 40 K/h, that protects the glass windows from improper thermal stress. Above 80 °C the heat transfer to the test section, tanks and piping as well as the increasing heat losses require more heating power. This demand was provided by steam heating, taking into account the minimal pressure level of 22 bar to avoid flashing. The necessary steam was supplied by the TOPFLOW steam generator circuitry (section 2.4 Operational measurement technique and calibration procedures) and adjusted by the steam controller FI4_09_SB (Fig. 8, App. 4). Using the large amount of condensation enthalpy an effective preheating of the water in the test section with an acceptable gradient is feasible up to the operating temperature. After activation of the steam heating the electrical heater W07 was switched off. During the last hour of preheating

the cooling water flow through the condenser W05 was started, process steam was directed to the RPV simulator and at the same time the level in this tank and in the test section was decreased. Thus the level in the B20A also decreased and the water overflow in B20B stopped with the consequence that the circulation pump P16 was switched off. Now a free cross-section between the steam inlet into B19 and the condenser W05 appeared and a steam/nitrogen mix flowed through the tanks and test section modules into the condenser. On its path the steam heated-up the inner surface of the test rig and also the fluid inside by slight condensation. The residual steam condensed in W05 and the non-condensable nitrogen was released through the equalizing pipe in the TOPFLOW pressure tank atmosphere.

The pressure increase in the TOPFLOW pressure tank was not stopped before the nominal value was exceeded by a few bar, if possible (maximal operation pressure of 50 bar). This allows a slight overheating of the test rig. If saturation condition was achieved, the heating steam supply (FI4_09_SB) was closed and the electrical heater W07 was switched on again to compensate heat losses. Then the system pressure and the injected water mass flow were adjusted to the nominal values. Furthermore, the water level in the B19 tank was decreased down to a level, significantly below the bottom edge of the horizontal test section module (unobstructed outflow condition) and the B20B tank level was regulated to the half-height of the steel sheet. Then the feeding- and release valves and also the ball valves in the drain pipes were closed. This operation allows an enclosed water inventory in the CCFL test rig that is a necessary condition for the application of mass balances for the data evaluation. Now the steam mass flow was increased to a value that allows a counter-current flow near the onset of flooding. The measurements were executed similar to the air-water tests, described above.

It is obvious, that the steam operation results in some specifics. So these tests ran at almost saturation condition. The water flowed through the circulation loops and slightly cooled down due to heat losses. This effect influenced the test condition as more as less water circulated. It was considered during data evaluation. A second source of abrupt temperature decrease was the moment, when the pump P16 was switched on, to regulate the level in B20B tank due to CCFL water overflow. The water volume in this tank was heated only less by partly condensation of residual steam over the time span from the completion of preheating (P16 switched off) to the reactivation of this circulation pump during the flooding CCFL operation. To minimize this unwanted process, after activation of the P16 the test conditions were kept constant for some time and the water temperature was increased by electrical heater W07 and steam condensation in the test section until the temperature in the P16 circulation loop was decreased up to an acceptable range.

Furthermore due to heat losses along the steam feeding pipe and from the test rig into the pressure tank atmosphere, steam condensed and the mass flow decreased. This process influenced on the one hand the steam volume flow through the test section and on the other hand the water balances in the RPV simulator and the SG separator. To consider this, the heat losses in the steam pipe and around the pressure tank were estimated and the parameters were corrected respectively.

The residual steam was condensed in W05. The condensate flowed down along the vertical heat exchanger pipes and collected at its bottom. The lower part of the condenser is connected to a condensate drain tank (Fig. 8) that is arranged below the pressure tank. So the condensate flowed into this tank through a gravity pipe. The limited volume flow through this pipe led to a condensate retention in the W05 if

high condensation capacity is necessary. To avoid problems with the gas equalizing pipe, a superimposed two-level controller opens the condensate drain valve to a higher level and releases a big amount of condensate discontinuously. This process leads to slight pressure fluctuations in the pressure tank. To avoid unwanted influence on the tests the data recording was done outside of these activities, if possible. For this reason the condensate mass flow was not used for data evaluation.

After the preheating procedure non-condensable gases could remain in the test section. For this reason a degasification pipe was installed on the RPV simulator opposite to the horizontal test module connection. Using this pipe a nitrogen/steam mixture could blow off from the tank. The test section and the SG simulator were degassed by the steam flow into the condenser with a maximum level in the tanks B20A and B20B. The complete degassing was verified by comparison of the saturation temperature as function of the tank pressure and the measured temperatures in the test rig. The non-condensable gases were removed on each steam operation day before the measurements were started and on demand.

Tab. 2 contains 3 pressure levels for steam tests. The 25 and 50 bar experiments were prepared as described above. In contrast, for 10 bar nominal pressure the test rig was heated-up by steam injection at a higher pressure level (22 bar) to avoid flashing. After a few K overheating related to the saturation temperature at nominal pressure, the steam heating was closed and the pressure was decreased down to the nominal value to start the measurements. At saturation or slightly sub-cooled condition the flashing risk is quite small, so the 10 bar tests were completed without damage of the glass windows.

As aforementioned the condenser W05 has a direct connection to the inner atmosphere of the TOPFLOW pressure tank through the equalizing pipe. So the humidity inside the tank is quite high and sometimes the glass windows, especially of the horizontal channel, tended to fog up at the bottom corners. This effect occurred at few image sequences nevertheless also in this cases the flow structure is visible.

5. Available data

5.1 Operational data

One important task of the current project was the presentation of the CCFL data in terms of Wallis parameter as a function of the pressure. For this, more than 100 operational data were recorded and stored in DIAdem data format with a frequency of 1 Hz. A list of all available parameters is attached to this report as App. 4. To allow a common access to this data, they were converted to MS Excel format and stored in single data sheets arranged in groups, related to the test series. Here the authors remember that a test series include all measurements with variable gas flow and constant pressure and injected water flow. So the data of each series was stored in a separate Excel file that additionally contains the following information:

- a complete listing of the test section dimensions as well as of pipe length and cross sections of the circulation loops for volume determination;
- one sheet with the geometry of the steam feeding pipe from the flow sensors FIC4-04/FIC4-05 to the injection point into the RPV simulator and an estimation of the condensate mass flow as function of the heat losses or the steam pressure respectively;
- a sheet with the geometrical parameter of the TOPFLOW pressure tank, both gas pipes and the heat exchanger of the nitrogen/air cooling system.

Beside this, the basic information is presented in the sheet "Wallis". Here all necessary parameters (averaged values, gradients, differences etc.) are combined with the thermal hydraulic properties, so that the Wallis parameter for gas and liquid flow can be calculated. Also the required correction and verification methods are included. Of course there are some differences in the data evaluation for air-water- and steam-water test series. Both data evaluation methods are described in detail in the following section. The thermal hydraulic properties of steam, water and humid air were determined by the IAPWS-IF97 or LibHuAir Excel plug-ins developed by the Hochschule Zittau Görlitz University of Applied Sciences. All Excel files are stored on the HZDR file server in a subfolder with the name "hot_leg_II\Diadem" in the file format: HS-II_CCFL_steam_$p$bar_$m$kgs.xlsx for steam-water tests and HS-II_CCFL_air_$p$bar_$m$kgs.xlsx for air-water tests. Thereby p stands for the pressure in bar and m for the injected water mass flow in kg/s. Additional a visualization of the non-dimensional superficial velocities and further evaluated data are included in the file "Overview.xlsx". The information about the slug frequencies evaluation is presented in the files: "HS_II_PI_fft_eval_rough.xlsx" and "HS_II_PI_fft_eval_fine.xlsx". The data on the server are backed up periodically to the HZDR central data tape archive, so that the data security is guaranteed.

5.2 Image data

According to section 3.1 Visual observation one high-speed camera and two web-cams were applied for the observation of flow structure in the CCFL test section. The first one captured image sequences with a frequency of 500 Hz over a time span of about 13 s. The frequency of 500 Hz and a spatial resolution of 1250 x 1250 pixels were selected to allow droplet or small bubble tracing methods, if necessary. During the measurement 6500 pictures were stored in the camera memory and then copied offline to the measurement PC as a compact file (*.raw3) after the trigger time. For the data analysis this raw3-file was unpacked and the single bmp-files were stored on the same server as the operational data. After completion of the image evaluation the

picture sequences were packed in zip-archives, one test in one archive. There are two subdirectories in the directory *hot_leg_II*: *tests_air* and *tests_steam.* There all files for each test are stored for air and steam flows respectively. In each folder a *bmp_images_sequences* subdirectory exists that contains the zip-archives as, e.g. CCFLnnn.zip with nnn as unique test number.

For the observation of the horizontal test section modules two web-cams were installed. Thereby the first one was positioned near the RPV simulator and the second – downstream, related to the gas flow. During the tests they recorded videos with a frequency of 60 Hz over a time of more than 1 minute. As reported in section 3.1 Visual observation the images of the web-cams were synchronized by 2 LEDs, whose signal was visible in both recorded picture sectors below the test section. The spatial resolution of the video images is 1280 x 720 pixels. The videos of the web-cams were saved with the aid of the H 264 codec that is available on the Internet. Using this codec and the video file single image sequences can be generated. The videos are stored in the associated test folder, e.g.: CCFLnnn_p_mmmm_FFF_up/down; nnn and p are described above, mmmm is the injected water mass flow in g/s and FFF – the air volume flow in m³/h (norm condition) or the steam mass flow in g/s. The authors point out that these values are nominal one. Up or down identify the flooding or deflooding character of the test. The video files labeled with the common string and an additional specification of the camera (cam1 or cam2) following by the letter *a*. The last one was added to select the data files in the case of test repetition, whereat *b* was used. Beside the video files the first and the last image of the video sequence are saved in the same folder and named by the video string with the adding *pre* and *post* respectively.

5.3 Data of the special pressure sensors

The current CCFL test rig was equipped with 6 pressure sensors (PI8-31 – PI8-36) along the horizontal test section modules to measure pressure fluctuations caused by slug flow. As described in section 3.3 Additional pressure measurement an external data logger was applied. It enables up to 48 analog input channels. So it was used not only for the 6 pressure sensors but also for the differential pressure of the LI8-05 (tank level of B20A), the pressure PI8-37 (inside the top part of B20) and the trigger signal (digital channel). The data logger requires a structuring of the input channels in groups of maximal 6 parameters. Hence the 6 test section pressures were united to the first group and the other values to a second one. The logger recorded the data from the start in the morning till switching off at the end of the operational day with a frequency of 1 Hz. During the trigger period the frequency was increased up to the maximum of 10 Hz. It provides the data in Excel *.csv format. So after completion of each test two data files (two groups) from the logger were copied to the measurement PC and the relevant parts were cut out and stored separately. These files include 600 pressure values for 1 minute trigger time as well as some pre and post data.

Each csv-file consists of several data columns. The first one contains a unique line number. Then the data and time information follows with a time resolution of a tenth of a second. Starting with the next column the data channels are stored. Since the first csv-file contains the 6 test section pressures in mbar, the second one provides the LI8-05, the PI8-37 (both in mbar) and the digital trigger signal. The first line in both files is a header that lists the names of the columns, including the dimension units. The csv-files are labeled by the common string added with the identifier

gruppe1 or *gruppe2* for the parameters of group one and two respectively. As the video sequences also these files are stored in the associated test directory.

The 10 Hz data in the files may be selected by the analysis of the time increment or by using of the trigger signal changing (1 for activated trigger) in the second file.

6. Data processing and evaluation

6.1 Processing of the operational data

The operational data was recorded over the entire measurement day with the TOPFLOW data acquisition system. The data fields associated to the single tests were marked by a trigger signal that is saved at the end of the operational data matrix. As aforementioned the test duration was fixed to 1 minute, whereat the thermal hydraulic parameters were kept constant for a time span of usually 10 minutes before the test was started. So, for the data evaluation a data field of all available parameters and 10 minutes including the trigger time was selected for each test, converted to Excel format, stored in a separate sheet and labeled with the corresponding test number. These data are the basis for the following evaluation procedures. As a first preparative step some important thermal hydraulic parameters were plotted against the test time:

- the two bottom temperatures in the RPV simulator tank B19 (TI8-32 & TI8-121),
- the same temperatures in the SG separator tank B20B (TI8-31 & TI8-117),
- 3 temperatures in the circulation loop (TI8-47, TI8-41 and TI8-48),
- the water levels in the B19 (LIC8-02) and in the B20B tanks (LIC8-01),
- the water mass flows at the pressure side of pump P18 (FIC8-42, from B19) and at the pressure side of pump P16 (FIC8-40, from B20B) as well as
- the mass flow of the injected water into the B20A (FI8-41).

The 8 graphs were arranged below the data matrix of each test point in the Excel file of the current test series. Based on these trends the quality of the test data was assessed. If all trends satisfied the desired characteristics, the entire period of 10 minutes was used for the further data processing. If problems appeared, the time span was reduced to the valid period. The beginning and the end of this period is indicated in the yellow marked field above the graphs. Using the valid time all required thermal hydraulic parameters were averaged and additionally the minimum and maximum were determined. In the following chapters always these time-averaged operational parameters are applied if no special indices or signs are given.

In opposite to the data evaluation procedure of the previous hot leg tests [1] the tank level measurements of the TOPFLOW PCS was used directly for the current data analysis, because their quality was improved significantly. In the following sections as the time-averaged levels as their gradients over the time were applied.

6.2 Flooding characteristics

As reported in [1] for a meaningful comparison of experimental data, the non-dimensional superficial velocity j^*_k (called Wallis parameter) is commonly used to plot the flooding diagram for the phase *k*. This parameter was defined by Wallis & Dobson [2] for near horizontal channels with rectangular cross-section as follows:

$$j_k^* = \frac{j_k}{\sqrt{g \cdot H}} \sqrt{\frac{\rho_{k,TS}}{\rho_{L,TS} - \rho_{G,TS}}} \qquad (2)$$

Here j_k is the superficial velocity of the phase k, g – the acceleration of gravity, H – the channel height and ρ - the density: with index k for the variable phase, L – for liquid and G – for gas as well as TS for test section.

The original equation of Wallis and Dobson includes the pipe diameter as characteristic geometrical parameter, because their test data was measured in circular pipes. In order to define the Wallis parameter for a horizontal channel with rectangular cross section, already for the previous hot leg tests [5] this length term was substituted by the duct height H. This also was done by Hihari et al. [3], who examined the slugging of counter-current gas-liquid flow in a horizontal rectangular channel. Furthermore, this way is supported by the experimental results of Zapke und Kröger [4], who investigated counter-current flows in inclined and vertical rectangular ducts. From experiments in channels with different rectangular cross sections, they concluded that the flooding gas velocity depends only on the height of the channel and not on its width.

Of course the calculation procedure of both Wallis parameters depends on the gas type, e.g. for steam tests condensation effects have to be considered. So it is reasonable to analyze the air- and the steam-water tests individually. The following data evaluation procedures correspond to the Excel sheets in the test series files. So the authors recommend comparing these explanations with the calculations on the *Wallis* sheet.

6.2.1 Air-water flow

The first task was the determination of the superficial gas velocity in the channel that is based on the injected air volume flow (V_{norm}). As reported in section 2.5 Inspection of the air flow meters FIC4-10 and FIC4-11 the measured air flow was corrected by the results of the comparative measurements with a rotameter. After this the norm flow (p = 1.01325 bar and t = 273.15 K) was recalculated to the operational condition in the test section (V_{TS}). For this purpose the thermal state equation for an ideal gas was used:

$$\dot{V}_{G,TS} = \dot{V}_{norm} \frac{p_{norm} \cdot T_{G,TS}}{p_{TS} \cdot T_{norm}} \qquad (3)$$

In equation (3) p specifies the pressure and T – the temperature in K, the index *norm* refers to normative- and *TS* to test section condition. The operational pressure in the test section was defined as average from the gas pressure in the inlet pipe (PI8-01) and in the pressure tank (PIC8-62), so the pressure drop along the test rig is considered. Since both pressure sensors measured relatively to the atmospheric pressure, it changes was corrected:

$$p_{TS} = \frac{(PI8-01) + (PIC8-62)}{2} - (p_{ps} - p_{at}), \qquad (4)$$

with p_{ps} as reference pressure of the pressure sensors (1 bar) and p_{at} as atmospheric pressure. The last one was obtained from the value at the sea level p_0 published hourly in the internet for the meteorological station Dresden-Klotzsche, which was converted to the altitude z of the HZDR (290 m) applying the barometric formula:

$$p_{at} = p_0 \cdot e^{-\frac{g \cdot M_{air}}{R \cdot T_{air}} \cdot z}, \qquad (5)$$

here M_{air} is the molar mass of air ($2.896*10^{-2}$ kg/mol) and R – the universal gas constant (8.314 J/(mol*K)). The temperature T_{air} was measured around the TOPFLOW pressure tank and is used in (5) in K.

The gas temperature in the test section ($T_{G,TS}$) is obtained as averaged value of 5 single measurements along the gas path through the test rig, namely TI8-63, TI8-04, TI8-124, TI8-125 and TI8-12 (Fig. 8).

Using the real air volume flow in the test section and the cross section area of the rectangular channel (A_{ch}) the air superficial velocity j_G was obtained:

$$j_G = \frac{\dot{V}_{G,TS}}{A_{ch}} \tag{6}$$

For the definition of the air Wallis parameter with eq. (2) the air and the liquid density are necessary. The first one was determined using the Excel add-in LibHuAir by the Hochschule Zittau Görlitz – University of Applied Science:

$$\rho_{G,TS} = f(p_{TS}, t_{G,TS}, xw_{air}), \tag{7}$$

with xw_{air} as air humidity in g/kg. The air humidity wasn't measured in the test section or in the blow-down air flow. The injected air is prepared on a compressor station of the HZDR with a dew point of -80 °C, so it can be considered as practically dry. On the path through the test section the humidity increased due to churn turbulent contact with the liquid phase. So the air density was calculated with a humidity fraction that corresponds to almost 50% relative moisture. Additionally, the influence of the air humidity to the density was investigated and resulted in a quite low density uncertainty.

The next step was the calculation of the liquid density that was done by the IAPWS-IF97 library also developed by the Hochschule Zittau Görlitz – University of Applied Science:

$$\rho_{L,TS} = f(p_{TS}, t_{L,TS}) \tag{8}$$

The liquid temperature in the test section $t_{L,TS}$ was determined in dependence on the water flow through the horizontal channel that was defined by the power of the pump P18. When it was in operation, the averaged value between the TS inlet and outlet temperature ($t^o_{L,TS}$) was used. In the opposite case only the inlet temperature ($t^i_{L,TS}$) was valid.

$$t^i_{L,TS} = \frac{(TI8-48)+(TI8-66)+(TI8-67)+(TI8-68)}{4} \tag{9}$$

The TS liquid outlet temperature depends on the level in the B19 tank:

$$t^o_{L,TS} = \frac{(TI8-121)+(TI8-32)+(TI8-47)}{3}, \quad \text{if LIC8-02} > 0.3 \text{ m;} \tag{10}$$

otherwise:

$$t^o_{L,TS} = \frac{(TI8-32)+(TI8-47)}{2}.$$

In this way the calculation of the air Wallis parameter is complete.

Next the algorithms for the definition of the liquid superficial velocity are descripted. Despite of the injected water mass flow, here only the discharged water flow is relevant. According to the test procedure the nominal water mass flow was injected

into the SG separator B20A. Depending on the counter-current gas volume flow a part of this water may restrain in the B20A and overflows over the steel sheet into the B20B tank. The other discharged part flows through the test section into the RPV simulator B19. As explained in section 4.2 Facility preparation and test procedure the liquid from both tanks (B19 and B20B) is returned to the tank B20A, so that the entire CCFL test rig may be regarded as a closed system. This approach allows the application of mass balances to determine the steam and liquid flows. Hence the discharge liquid mass flow (m_{dis}) was defined as sum of the released water mass flow (m_{rel}) from the tank and the mass changing (dm^{dis}_{tank}) inside it.

$$\dot{m}_{dis} = \dot{m}_{rel} + \dot{dm}^{dis}_{tank} \tag{11}$$

Furthermore, this parameter can be calculated directly, using the balance in the RPV simulator B19 and indirectly as a difference between the injected water mass flow and the balance in the SG separator B20B. Both methods were applied to increase the accuracy of the results. Firstly the procedure with the B19 tank is explained. The released water mass flow was measured by the Coriolis flow meter FIC8-42 at the pressure side of the pump P18. Since also the Coriolis devices have uncertainties the FIC8-42 was adjusted to the FI8-41 (injected water). Each test series includes counter-current flow tests without limitation. Hence the entire injected water circulated through the test section into the B19 and returned to the tank B20A by the pump P18 (P16 was switched off). This case was used to correlate the values of both flow meters that resulted in an offset for FIC8-42. The FI8-41 was defined as reference device, because the correlation is also necessary for the parallel procedure with the B20B tank and the FIC8-40. In this way the FI8-41 is a link between both parallel procedures and an averaging of the results makes sense. Due to the fact that the zero point of all three flow meters is valid, the measured mass flow values of FIC8-42 were corrected by a linear function, determined between the zero point and the maximal value (offset). The corrected mass flow results in:

$$(\dot{FIC8} - 42)_{cor} = (\dot{FIC8} - 42)_{meas} \cdot \frac{\sum_{i=1}^{n}(\dot{FI8} - 41)_i}{\sum_{i=1}^{n}(\dot{FIC8} - 42)_i} \tag{12}$$

In (12) the index cor means corrected value, meas – measurement and i – the selected test for correlation, if both mass flow sensors works serially. If more than one correlation test is available (n > 1), averaged values were used in (12) for both mass flows (i) to increase the accuracy of the correction coefficient. In this way the 1st component of the discharged water flow according to (11) was determined.

Further the mass gradient (dm^{dis}_{tank}) of the water in the B19 tank can be defined as:

$$\dot{dm}^{dis}_{tank} = \dot{dV}^{dis}_{tank} \cdot \bar{\rho}_{L,tank}, \tag{13}$$

here dV^{dis}_{tank} is the volume changing of the liquid in the tank and $\rho_{L,tank}$ the time averaged liquid density inside it, that is obtained as:

$$\bar{\rho}_{L,tank} = f(p_{TS}, \bar{t}_{L,tank}) \tag{14}$$

In eq. (14) the averaged liquid temperature in the B19 tank is determined as:

$$\bar{t}_{L,B19} = \frac{(TI8-32) + (TI8-121) + (TI8-122)}{3} \quad \text{if LIC8-02} > 0.53 \text{ m or} \tag{15}$$

$$\bar{t}_{L,B19} = \frac{(TI8-32)+(TI8-121)}{2} \quad \text{if } 0.53 \text{ m} \geq \text{LIC8-02} > 0.3 \text{ m or}$$

$$\bar{t}_{L,B19} = (TI8-32) \quad \text{if LIC8-02} \leq 0.3 \text{ m}.$$

In eq. (15) the liquid level limits for the definition of $t_{L,tank}$ are selected in such a way, that the liquid level in the tank was minimal 2 cm above the highest thermocouple. So it is ensured that also the highest TC measures the liquid temperature.

A closer examination of the test procedure reveals that the complete volume changing (dV_{tank}) consists not only of the residual part of the discharged water flow (dV^{dis}_{tank}) but also of the temperature-dependent volume changing of the liquid as in the tank itself (dV^t_{tank}) as in the connected circulation loop (dV^t_{circ}), so:

$$\dot{V}_{tank} = d\dot{V}^{dis}_{tank} + d\dot{V}^t_{tank} + d\dot{V}^t_{circ} \quad \text{or} \tag{16}$$

$$d\dot{V}^{dis}_{tank} = d\dot{V}_{tank} - d\dot{V}^t_{tank} - d\dot{V}^t_{circ}$$

For the further data evaluation it is necessary to assume that the CCFL tests were operated under steady state condition according to the liquid and gas flows, the pressure and to the flow regime, but not completely regarding to the temperature. For this reason in the test data two temperature levels were defined: at the beginning (*_1) and at the end (*_2) of the test, as averaged values over 10 s after the test start and before the test end respectively.

The connected to tank B19 circulation loop is composed of pipe 104, pump P18, pipe 142, steam heater M03, pipe 147, electrical heater W07, pipe 153 and tank B20A. (see Fig. 8 and App. 5). It is equipped with several temperature measurements which were used for the determination of the temperature-dependent volume changings. Thus the entire circulation loop was divided in 3 parts. The following list assigns the single volume parts to the corresponding temperature measurement:

- pipe 104 and pump P18 – TI8-32,
- pipe 142, steam heater M03, pipe 147, electrical heater W07 and pipe 153 – averaged value of TI8-47 and TI8-48 as well as
- tank B20A – averaged value of TI8-66 and TI8-67.

The geometrical dimensions for the volume determination of these 3 parts are presented in the sheet *geometry* included in all Excel test files.

So the temperature-dependent liquid volume changing of the entire circulation loop was obtained as:

$$d\dot{V}^t_{circ} = d\dot{V}^t_{104} + d\dot{V}^t_{M03} + d\dot{V}^t_{B20A} \tag{17}$$

Next the single dV^t_k contents were defined based on the assumption that the entire circulation loop volume is completely filled with incompressible water. So a temperature changing leads to a volume changing that depends on the density gradient. Further the volume changing between the temperature levels 1 and 2 is related to the entire valid test period. Thus for dV^t_k follows:

$$d\dot{V}^t_k = \frac{V_k \cdot (\rho_{L,k,1} - \rho_{L,k,2})}{\rho_{L,k,2} \cdot (\tau_1 - \tau_2)} \tag{18}$$

In eq. (18) the index k stands for the tank B19 or the single loop parts. V specifies its volume, ρ_L - the liquid density and τ - the absolute time. The indices 1 and 2 related to the start or end of the test period respectively. Both liquid densities of each loop part defined as:

$$\rho_{L,k,j} = f(p_{TS}, t_{L,k,j}), \qquad (19)$$

with t_L as liquid temperature and index j as marker for the start or end time of the test.

Now the specifics of the single loop parts are explained. The first one is the RPV simulator B19. Here the corresponding temperature $t_{L,B19,j}$ is determined in dependence on the liquid level in the tank LIC8-02:

$$t_{L,B19,j} = \frac{(TI8-32)_j + (TI8-121)_j}{2}, \quad \text{if LIC8-02} > 0.3 \text{ m} \qquad (20)$$

otherwise:

$$t_{L,B19,j} = (TI8 - 32)_j$$

The liquid volume V_{B19} is calculated as the time averaged level in the tank (LIC8-02) multiplied by the inner cross section area $A_{cs,tank}$:

$$V_{B19} = \bar{L}_{B19} \cdot A_{cs,B19} \qquad (21)$$

The corresponding temperatures of the circulation loop parts are indicated in the list above. The volumes V_{104} and V_{M03} are determined with the information at the *geometry* sheet in the Excel files. V_{B20A} is estimated using a constant middle liquid level in the tank and the inner cross-section. The constant level has to be applied, because the differential pressure sensor of the level measurement was damaged during the pressure changings in the TOPFLOW pressure tank. Nevertheless this approach is valid, because the nominal water flow was injected into the B20A tank, so that it always was filled up to a minimal level of more than 0.86 m (lower bend of the SG inlet chamber module). A 2nd level fixed-point is the height position of the overflow edge of the steel sheet in the B20 tank at about 1.1 m that may achieve during CCFL or zero penetration point. As a good compromise a liquid level value of 0.98 m was used. An additional feature of the calculation of dV^t_{M03} and dV^t_{B20A} results from the parallel operation of the RPV simulator and the SG separator. So the temperature-dependent volume changing in the 2nd and 3rd loop part influences as dV_{B19} as dV_{B20B}. To consider this effect the dV^t_k (k = M03 or B20A) calculation in accordance to eq. (18) is completed with a mass flow weighting:

- RPV simulator B19: FIC8-42 / FI8-41 and
- SG separator B20B: FIC8-40 / FI8-41.

The next step is the definition of dV_{B19} according to eq. (16). This term corresponds to the real liquid level gradient in the tank B19 (dL_{B19}). It is obtained as follows:

$$\dot{V}_{B19} = \dot{L}_{B19} \cdot A_{cs,B19} \qquad (22)$$

DL_{B19} is the slope of the LIC8-02 characteristic.

In this way all necessary information are prepared to calculate dV^{dis}_{tank} according to eq. (16), the corresponding dm^{dis}_{tank} with eq. (13) and m_{dis} according to eq. (11).

Therefore the 1st direct method of m_{dis} definition with the RPV simulator B19 is almost completed.

As reported above the enclosed CCFL test rig opens the possibility to calculate m_{dis} by a 2nd indirect method using the SG simulator tank B20B. The calculation procedure of this method is similar to the first, so that it is not repeated here completely. Only the differences with reference to the corresponding equations are presented in the following paragraphs.

The measurement of the released water flow from the tank B20B is done by the Coriolis mass flow meter FIC8-40. So the mass flow correction according to eq. (12) is done by the operational parameter FIC8-40 and FI8-41. In this case for the definition of the correction coefficient all tests (n) with switched off pump P18 were applied.

For the definition of the time averaged liquid density in the tank B20B (analog to tank B19 eq. (14) and (15)) $t_{L,B20B}$ was obtained as:

$$\bar{t}_{L,B20B} = \frac{(TI8-31)+(TI8-117)+(TI8-118)}{3} \quad \text{if LIC8-01 > 0.72 m or} \qquad (23)$$
$$\bar{t}_{L,B20B} = \frac{(TI8-31)+(TI8-117)}{2} \quad \text{if 0.72 m ≥ LIC8-01 > 0.42 m or}$$
$$\bar{t}_{L,B20B} = (TI8-31) \quad \text{if LIC8-01 ≤ 0.42 m.}$$

The next difference consists in the composition of the circulation loop around the SG separator tank. In this case the loop includes the following components with their corresponding temperatures:

- pipe 101 and pump P16 - TI8-31,
- pipe 141 (partly), pipe 145, pipe 142 (partly), steam heater M03, pipe 147, electrical heater W07 and pipe 153 – averaged value of TI8-47 and TI8-48 as well as
- tank B20A - averaged value of TI8-66 and TI8-67.

Accordingly, equation (17) changes to:

$$\dot{V}_{circ}^{t} = \dot{V}_{101}^{t} + \dot{V}_{M03}^{t} + \dot{V}_{B20A}^{t} \qquad (24)$$

Further the index k in eq. (18) and (19) starts with the B20B tank, followed by pipe 101 and so on. Also eq. (20) changed to:

$$t_{L,B20B,j} = \frac{(TI8-31)_j+(TI8-117)_j+(TI8-118)_j}{3} \quad \text{if LIC8-01 > 0.72 m or} \qquad (25)$$
$$t_{L,B20B,j} = \frac{(TI8-31)_j+(TI8-117)_j}{2} \quad \text{if 0.72 m ≥ LIC8-01 > 0.42 m or}$$
$$t_{L,B20B,j} = (TI8-31)_j \quad \text{if LIC8-01 ≤ 0.42 m.}$$

and eq. (21) with respect to tank B20B:

$$V_{B20B} = \bar{L}_{B20B} \cdot A_{cs,B20B} \qquad (26)$$

Naturally the calculation of dV_{B20B} results in:

$$\dot{V}_{B20B} = \dot{L}_{B20B} \cdot A_{cs,B20B} \qquad (27)$$

43

with dL_{B20B} as slope of the LIC8-01 measurement.

Now all parameters for the definition of m_{dis} (eq. 11) regarding the tank B20B are available that results in an equal data evaluation level for both tanks.

The next step is a comparison of the change of mass in both tanks. The boundary condition of a complete enclosed CCFL test rig and the correction of the temperature-dependent volume changings lead to the conclusion:

$$\dot{dm}_{B19}^{dis} + \dot{dm}_{B20B}^{dis} = \Delta \dot{dm}^{dis} = 0, \tag{28}$$

here Δdm^{dis} specifies the deviation between the mass gradients defined using both tanks.

Thus a control of the evaluation results is possible. In the reality eq. (28) results in slight negative values in the range of -5 till -1 g/s. This deviation might be caused by residual uncertainties of the temperature-dependent volume corrections or by minor leakages through the floating-ring type shaft seal of the pumps P16 or P18. The main reason is certainly the increasing humidity of the air flow through the test section, beginning with dry air on the injection - up to maximal 100 % relative humidity (assumption) in the blow off pipe takes away up to 3 g/s liquid according to the gas volume flow. The influence of the air moisture was estimated in the Excel files for the air-water tests at the end of the *Wallis* sheet.

Despite the reasons, the residual deviation was used for a correction of both mass gradients. Similar to the definition of the temperature-dependent volume changings for the common parts of the circulation loops, the ratio of the corresponding mass flows was used:

$$\dot{dm}_{B19}^{dis,c} = \dot{dm}_{B19}^{dis} - \Delta \dot{dm}^{dis} \cdot \frac{(FIC8-42)}{(FI8-41)} \tag{29}$$
$$\dot{dm}_{B20B}^{dis,c} = \dot{dm}_{B20B}^{dis} - \Delta \dot{dm}^{dis} \cdot \frac{(FIC8-40)}{(FI8-41)},$$

with c – for corrected value.

Using the corrected mass flows and gradients the CCFL discharged mass flow can be obtained according to eq. (11) as:

$$\dot{m}_{B19}^{dis} = (\dot{FIC8-42})_{cor} + \dot{dm}_{B19}^{dis,c} \tag{30}$$
$$\dot{m}_{B20B}^{dis} = (\dot{FI8-41}) - ((\dot{FIC8-40})_{cor} + \dot{dm}_{B20B}^{dis,c})$$

Now both tank-dependent discharged mass flows can be averaged:

$$\dot{m}_{TS}^{dis} = \frac{\dot{m}_{B19}^{dis} + \dot{m}_{B20B}^{dis}}{2} \tag{31}$$

The discharged volume flow through the test section is calculated as:

$$\dot{V}_{TS}^{dis} = \frac{\dot{m}_{TS}^{dis}}{\rho_{L,TS}}, \tag{32}$$

here $\rho_{L,TS}$ is used as calculated according to eq. (8). The next-to-last step is the definition of the liquid discharged water superficial velocity j_L:

$$j_L = \frac{\dot{V}_{TS}^{dis}}{A_{ch}} \tag{33}$$

Using j_L from the last equation and the densities defined in eq. (7) and (8) the liquid Wallis parameter can be calculated according to eq. (2). For visualization commonly the square root of the non-dimensional superficial velocities j_k^* is used, so it was calculated at the end of the data table in the Excel *Wallis* sheets. As a preliminary overview all Wallis parameters of the current test series are plotted below the data table.

Due to measurement and data evaluation uncertainties j_L^* for the zero penetration point are afflicted with noise that results in maximal fluctuations of ± 1 g/s discharged liquid flow. Especially the negative values make problems under the square root. Fortunately the complete CCFL condition at the zero penetration point was checked by observation of the flow structure in the last horizontal TS module downstream related to the discharge liquid flow (see section 4.2 Facility preparation and test procedure and Fig. 13). Thus, j_L^* was set to zero for all tests with positive observation results. This is the case for all test series except one air-water series at 2 bar and 1 kg/s injected water mass flow. There zero penetration condition was not achieved and the CCFL j_L^* value was kept unchanged as defined.

6.2.2 Steam-water flow

In principle the definition of the non-dimensional superficial gas and liquid velocities for the steam-water tests was done similar to the air-water flows. This concerns the calculation of the discharged water mass flow according to eq. (11) using both tanks B19 and B20B. Of course, there are some features based on the unitary system of steam and saturated water that leads to high temperatures with heat losses and steam condensation effects.

Also for these tests j_k^* has to be obtained in consideration with eq. (2). Therefore, beside j_k the liquid and the steam densities are necessary that require the pressure (p_{TS}) and both temperatures inside the test section. Due to a significant higher pressure level inside it, the influence of the atmospheric pressure is neglected in this case. Thus, p_{TS} was calculated as:

$$p_{TS} = \frac{(PI8-01)+(PIC8-62)}{2} \tag{34}$$

This approach uses a pressure sensor upstream (PI8-01) and one downstream (PIC8-62) the test rig and provides an averaged value for the test rig under consideration of its pressure drop.

As gas temperature the saturation temperature at the current pressure level is used, since the TOPFLOW steam generator supplies saturated steam (see section 2.4 Operational measurement technique and calibration procedures) and the pressure drop along the main steam pipe leads to an increase of the kinetic energy and not to superheated steam:

$$t_{G,TS} = t_S = f(p_{TS}) \tag{35}$$

Using the IAPWS-IF97 water property library of the *Hochschule Zittau-Görlitz University of Applied Science* the steam density can be obtained as:

$$\rho_{G,TS} = \rho'' = f(p_{TS}) \tag{36}$$

45

The liquid density $\rho_{L,TS}$ is defined according to eq. (8) and the necessary $t_{L,TS}$ with eq. (9 and 10) depending on the function of pump P18 respectively. However, due to uncertainties of the temperature measurements the value of $t_{L,TS}$ can occur above the saturation temperature and hence the liquid density fails. To avoid this, the density is defined according to the relation of the liquid test section temperature to the saturation temperature:

$$\rho_{L,TS} = \rho'_{L,TS} = f(p_{TS}), \quad \text{if} \ \ t_{L,TS} \geq t_S \tag{37}$$

$$\rho_{L,TS} = f(p_{TS}, t_{L,TS}), \quad \text{if} \ \ t_{L,TS} < t_S$$

This procedure is used not only for the liquid test section density but also for ρ_L in both tanks B19 and B20B.

The next step is the determination of j_G. The steam flow is measured as mass flow by 2 in series installed restrictor measuring (typ Rosemount 3095), which values are averaged:

$$\dot{m}_{G,TS} = \frac{(FI1-02) + (FIC4-04)}{2} \tag{38}$$

Between the flow meters and the injection point into the RPV simulator the steam flows through DN100 pipes of about 26 m length. The operating temperature in the steam pipes depends on the nominal pressure and is in a range of 180 to 264 °C. Hence, heat losses (Q^{pipe}) were considered and the waste condensation rate (m^{pipe}_{cond}) was estimated for steady state heat conduction:

$$\dot{m}^{pipe}_{cond} = \frac{\dot{Q}^{pipe}}{(h''_{H2O} - h'_{H2O})}, \tag{39}$$

where h''_{H2O} and h'_{H2O} are the enthalpies of saturated steam and saturated water as function of the steam pressure respectively. In this case a sub-cooling of the condensate in the steam pipe was not considered.

The heat loss Q^{pipe} was calculated according to [6] as follows:

$$\dot{Q}^{pipe} = \frac{\pi \cdot (t_S - t_{air}) \cdot L}{\frac{1}{\alpha_{cond} \cdot d^{pipe}_i} + \frac{1}{2 \cdot \lambda_{steel}} \cdot \ln \frac{d^{pipe}_o}{d^{pipe}_i} + \frac{1}{2 \cdot \lambda_{insu}} \cdot \ln \frac{d^{insu}_o}{d^{pipe}_o} + \frac{1}{\alpha_{out} \cdot d^{insu}_o}} \tag{40}$$

In eq. (40) t_{air} is the ambient temperature in the test building (was assumed to 20 °C), L – the length of the steam pipe, α – the heat transfer coefficient, λ - the thermal conductivity and the indices $_{cond}$ – condensation at the inner pipe wall, $_i$ – inner, $_o$ – outer, $_{insu}$ – thermal insulation and $_{out}$ – outer side of the thermal insulation. The denominator represents the entire thermal resistivity (R_Σ) of the insulated pipe. Its main part causes the thermal insulation. Further the heat transfer coefficient at the inner pipe wall is very high due to a high steam velocity, a turbulent flow regime and condensation effects. So the first term of R_Σ was neglected, also because the large calculation effort for heat losses estimation is unjustifiable. The temperature-dependent thermal conductivities for stainless steel and mineral wool were selected in [6]. The insulation limitations due to flanges, elbows and valves were considered by allowance of the pipe length according to [6]. The heat transfer coefficient at the outer surface of the pipe insulation for inactive air was estimated roughly by an empirical formula also according to [6] as:

$$\alpha_{out} = 8 + 0,04 \cdot (t^{insu}_o - t_{air}) \ \text{in [W/(m²K)]} \tag{41}$$

In the equation above t_o^{insu} is the surface temperature at the outer side of the thermal insulation. It was calculated iteratively using R_Σ without the first and last term in combination with eq. (40 and 41). The estimation results in the following condensation rates: 4 g/s (50 bar), 3 g/s (25 bar) and 2 g/s (10 bar). The calculations are presented at the Excel sheet *QI steam pipe* in all steam test files.

A further source of waste condensation results from the RPV simulator tank B19 and from the test section due to heat losses (a) as well as from the heat-up of the discharged water in the test section (b). The first part (a) is obtained by estimation of the heat losses through the CCFL test rig into the TOPFLOW pressure tank B04 (Q^{tr}) and further in the ambient air of the test building. Thereby the heat storage capacity of the nitrogen gas inside B04 and in the circulation cooling system (Q^{N2}_{cap}), the heat transfer from the nitrogen gas through the inner surface area to the tank B04 (Q^{N2-B04}_{trans}), the heat storage capacity of the tank steel (Q^{B04}_{cap}), the heat transfer from the outer surface area of B04 to the ambient air ($Q^{B04-air}_{trans}$) and the heat transfer of the circulation cooling system (Q^{W06}) were estimated:

$$\dot{Q}^{tr} = \dot{Q}^{N2}_{cap} + \dot{Q}^{N2-B04}_{trans} + \dot{Q}^{W06} \tag{42}$$

$$\dot{Q}^{N2-B04}_{trans} = \dot{Q}^{B04}_{cap} + \dot{Q}^{B04-air}_{trans} \tag{43}$$

Q^{N2}_{cap} was obtained by:

$$\dot{Q}^{N2}_{cap} = \frac{m^{N2} \cdot c_p^{N2} \cdot (t_i^{N2} - t_{i-1}^{N2})}{(\tau_i - \tau_{i-1})} \tag{44}$$

In eq. (44) m^{N2} is the mass of the entire nitrogen volume in the B04 (V_{B04}) and in the circulation cooling system (V_{W06}), driven by the fan V02. The content of both parts was calculated at the Excel sheet *QI B04*. So the mass is defined using the nitrogen density ρ^{N2}:

$$m^{N2} = \rho^{N2} \cdot (V_{B04} + V_{W06}) \tag{45}$$

$$\rho^{N2} = f((PIC8 - 62), t_i^{N2}, xw^{N2}) \tag{46}$$

The average temperature of the nitrogen was calculated as average of the outlet and inlet temperature of W06:

$$t_i^{N2} = \frac{(TI8-03)_i + (TI8-05)_i}{2} \tag{47}$$

The nitrogen humidity xw^{N2} was selected in such a way that the relative humidity was in a range of 95 – 100 %. It seems correct because during steam operation the moisture in the B04 permanently increased due to gas fluctuation through the pressure compensation pipe of the condenser W05.

Beside it, eq. (44) contains the isobaric specific heat capacity c_p^{N2} that was defined as:

$$c_p^{N2} = f((PIC8 - 62), t_i^{N2}, xw^{N2}) \tag{48}$$

Further the averaged nitrogen temperature t_i^{N2} and t_{i-1}^{N2} were determined by eq. (47) as time averaged value over the valid measurement time of the previous (i-1) and current (i) tests. The temperature of the previous test before test 1 was assumed according to the first tests. Finally the time span between both relevant tests ($\tau_i - \tau_{i-1}$) was obtained as the difference between both averaged absolute time values:

$$\tau_k = \frac{\tau_{k,1} + \tau_{k,2}}{2}, \text{ with k [i and i-1]} \tag{49}$$

In eq. (49) $\tau_{k,1}$ and $\tau_{k,2}$ are the start and the end of the valid measurement time of the k test. Similar to the nitrogen temperature also the time span for the first test ($\tau_1 - \tau_0$) was assumed.

The heat transfer from the nitrogen gas into the B04 tank is defined by:

$$\dot{Q}_{trans}^{N2-B04} = \alpha^{N2-B04} \cdot A_{in}^{B04} \cdot (t_i^{N2} - t_{Ain}^{B04}) \tag{50}$$

Here $\alpha^{N2\text{-}B04}$ is the heat transfer coefficient between the nitrogen and the B04 steel wall, A_{in}^{B04} – the inner surface area of the pressure tank B04 and t_{Ain}^{B04} – the temperature at the inner surface of B04. A_{in}^{B04} was integrated over the single areas of the pressure tank by a CAD program. This and the other necessary geometric values are presented at the Excel sheet *QI B04*.

For the estimation of the heat transfer coefficient the geometry of the CCFL test section and the TOPFLOW pressure tank B04 were simplified to a horizontal annular gap. The heat transfer through it was assumed as free convection. The last assumption is valid because the amount of forced convection due to the nitrogen circulation trough the tank is less by reason of the big tank cross section. Furthermore, the nitrogen density differences due to the injection of cooled gas into the tank lead to a fall down below the injection pipe, so that a very complex flow of nitrogen appears in the tank. Thus, the heat transfer coefficient according to [7] results in:

$$\alpha^{N2-B04} = \frac{Nu^{N2-B04} \cdot \lambda^{N2}}{l_{ch}} \tag{51}$$

Eq. (51) uses $Nu_{N2\text{-}B04}$ as Nusselt number for the heat transfer from the nitrogen to the B04 wall, λ^{N2} – thermal conductivity of the fluid and l_{ch} – as characteristic length, in this case the length of oncoming flow. The thermal conductivity was defined with the property library of humid air as follows:

$$\lambda^{N2} = f((PIC8 - 62), t_i^{N2}, xw^{N2}) \tag{52}$$

The characteristic length was calculated as difference between the inner radius of the cylindrical part of the TOPFLOW pressure tank (r_{in}^{B04}) and the outer radius of the CCFL test rig (r_{out}^{TS}). The last one was estimated as sum of the length-weighted hydraulic diameter of the RPV simulator B19, the horizontal and the inclined parts of the test section and the SG separator B20. The hydraulic diameters were calculated with outer dimensions under consideration of the thermal insulation:

$$l_{ch} = r_{in}^{B04} - r_{out}^{TS} \tag{53}$$

$$r_{out}^{TS} = 0.5 \cdot (d_{hyd}^{B19} \cdot \frac{L^{B19}}{L^{sum}} + d_{hyd}^{TS,hor} \cdot \frac{L^{TS,hor}}{L^{sum}} + d_{hyd}^{TS,inc} \cdot \frac{L^{TS,inc}}{L^{sum}} + d_{hyd}^{B20} \cdot \frac{L^{B20}}{L^{sum}}) \tag{54}$$

$$L^{sum} = \sum_{k=1}^{4} L^k, \; k \; [B19; \text{horizontal TS; inclined TS; B20}]$$

$$d_{hyd}^k = 4 \cdot \frac{H_k \cdot W_k}{2 \cdot (H_k + W_k)}, \text{ with H and W - as height and width respectively.}$$

Finally the Nusselt number was estimated in accordance to [7] as:

$$Nu^{N2-B04} = 0.2 \cdot Ra^{0.25} \cdot (\frac{r_{in}^{B04}}{r_{out}^{TS}})^{0.5} \tag{55}$$

$$Ra = Gr \cdot Pr \tag{56}$$

$$Gr = \frac{g \cdot l_{ch}^3 \cdot \beta_{N2} \cdot (t_{\tau,i}^{N2} - t_{Ain}^{B04})}{\nu_{N2}^2} \tag{57}$$

48

$$Pr = f((PIC8 - 62), t_i^{N2}, xw^{N2}) \tag{58}$$

In eq. (57) β_{N2} stands for the coefficient of thermal expansion of nitrogen that was selected according to [7] and ν_{N2} is the kinematic viscosity of nitrogen defined as:

$$\nu_{N2} = f((PIC8 - 62), t_i^{N2}, xw^{N2}) \tag{59}$$

Thus the 2nd term of eq. (42) $Q^{N2\text{-}B04}_{trans}$ can be obtained with eq. (50).

The 3rd term in eq. (42) is Q^{W06}. The heat exchange capacity of the circulation cooling system with W06 was taken directly from the TOPFLOW PCS where it is calculated with a frequency of 3 Hz. Q^{W06} is defined as follows:

$$\dot{Q}^{W06} = \dot{m}_{N2}^{W06} \cdot c_p^{N2} \cdot ((TI8 - 05) - (TI8 - 03)) \tag{60}$$

The nitrogen mass flow (m_{N2}^{W06}) in the equation above results from:

$$\dot{m}_{N2}^{W06} = \dot{V}_{N2}^{W06} \cdot \rho_{N2} \tag{61}$$

ρ_{N2} was used in accordance with eq. (46) and the nitrogen volume flow (V_{N2}^{W06}) was calculated from a differential pressure measurement of a Torbar sensor in the circulation pipe. The isobaric specific heat capacity c_p^{N2} was calculated according to eq. (48).

In eq. (50 and 57) the temperature of the inner surface of B04 (t^{B04}_{Ain}) was used. To get it, the heat-up of the B04 steel can be estimated, knowing the heat that remains in the tank material Q_{cap}^{B04}. From eq. (43) follows:

$$\dot{Q}_{cap}^{B04} = \dot{Q}_{trans}^{N2-B04} - \dot{Q}_{trans}^{B04-air}, \tag{62}$$

Similar to eq. (50) the heat release from the outer surface of B04 to the ambient air ($Q_{trans}^{B04\text{-}air}$) results to:

$$\dot{Q}_{trans}^{B04-air} = \alpha^{B04-air} \cdot A_{out}^{B04} \cdot (t_{Aout}^{B04} - t_i^{air}) \tag{63}$$

In eq. (63) $\alpha^{B04\text{-}air}$ is the heat transfer coefficient between the outer surface of the tank B04 and the ambient air, A^{B04}_{out} – the outer surface area of B04, t^{B04}_{out} – the temperature at the outer surface and t^{air}_i – the temperature of the ambient air.

The TOPFLOW pressure tank B04 was made of unalloyed steel (1.0580) with good heat conductivity (λ_{steel}) of about 54 W/(m*K). Taking into account a maximum heat emission of B04 of about 2 kW for the 50 bar tests and the large surface area of about 61 m² the temperature difference between the inner and outer tank surface can be determined for an equivalent cylindrical geometry according to [6] as:

$$t_{Aout}^{B04} - t_{Ain}^{B04} = \frac{\dot{Q}^{B04} \cdot \frac{1}{\lambda_{steel}} \cdot \ln(\frac{r_{out}^{B04}}{r_{in}^{B04}})}{2 \cdot \pi \cdot l_{cyl}^{B04}} \tag{64}$$

In eq. (64) Q^{B04} is the heat flow through the tank material that was set to the maximum heat emission of the outer surface and l^{B04}_{cyl} – the length of an area equivalent cylinder:

$$l_{cyl}^{B04} = \frac{\frac{(A_{out}^{B04} + A_{in}^{B04})}{2}}{2 \cdot \pi \cdot \frac{(r_{out}^{B04} + r_{in}^{B04})}{2}} \tag{65}$$

Appling both equations the temperature difference was estimated to 0.02 K and was neglected in the heat loss estimation. Hence the inner and outer surface temperatures were assumed equally. For the estimation of the heat flows and Gr-

numbers in eqs. (50, 57, 63 and 72) for the 1 test of a series $t^{B04}_{Aout} = t^{B04}_{Ain}$ was assumed regarding to the heat-up procedure of the CCFL test rig.

Furthermore the ambient temperature in the test building was not measured. Due to the small heat flows it was assumed as constant value of 18 °C for the 10 bar tests (Q_{max}: 0.5 kW) and 20 °C for the 25 bar tests with Q_{max} of 1.1 kW. By reason of the slightly higher heat flow for the 50 bar tests (Q_{max}: 2 kW) a linear increase of the ambient temperature was considered from 25 °C to 30 °C during the entire experimental day. For the assumption of t^{air}_i the meteorological condition of the experimental days was considered.

As in eq. (50) the inner surface area also the outer surface area in eq. (63) A^{B04}_{out} was added by a CAD program and is presented at the Excel sheet *QI B04*. In this case a consideration is reasonable because the difference between both surface areas is about 10 %.

So in eq. (63) remains the heat transfer coefficient that was estimated similar to eq. (51) as:

$$\alpha^{B04-air} = \frac{Nu^{B04-air} \cdot \lambda^{air}}{l_{ch}}, \tag{66}$$

here λ^{air} was determined as:

$$\lambda^{air} = f\left(1\ bar, t^{air}_i, xw^{air}\right), \tag{67}$$

with xw^{air} as air humidity that corresponds to a relative humidity of about 50 %. $Nu^{B04-air}$ and l_{ch} were estimated in accordance to [7] for free convection around a horizontal cylinder:

$$l_{ch} = \frac{\pi}{2} \cdot d^{B04}_{out} \tag{68}$$

$$Nu^{B04-air} = (0.752 + 0.387 \cdot \left[Ra \cdot f_3(Pr^{air})\right]^{1/6})^2 \tag{69}$$

$$f_3(Pr) = \left[1 + \left(\frac{0.559}{Pr^{air}}\right)^{9/16}\right]^{-16/9} \tag{70}$$

$$Pr^{air} = f\left(1\ bar, t^{air}_i, xw^{air}\right) \tag{71}$$

The Ra number was defined in accordance to eq. (56). Similar to eq. (57) the Gr number results to:

$$Gr = \frac{g \cdot l^3_{ch} \cdot \beta_{air} \cdot (t^{air}_i - t^{B04}_{Aout})}{\nu^2_{air}} \tag{72}$$

$$\beta_{air} = \frac{1}{(t^{air}_i + 273\ K)} \tag{73}$$

Finally the kinematic viscosity was defined by the property library for humid air as:

$$\nu_{air} = f\left(1\ bar, t^{air}_i, xw^{air}\right) \tag{74}$$

In this way the heat flow accumulated in the B04 steel Q^{B04}_{cap} may be estimated according to eq. (62). Using the last one and the time span between two successive tests the heat-up of the B04 tank can be calculated similar to eq. (44) as:

$$t^{B04}_i = t^{B04}_{i-1} + \frac{\dot{Q}^{B04}_{cap} \cdot (\tau_i - \tau_{i-1})}{m^{B04} \cdot c^{B04}_p} \tag{75}$$

In eq. (75) t^{B04}_i and t^{B04}_{i-1} are the average temperatures in the B04 steel for i and i-1 test. The time span $\tau_i - \tau_{i-1}$ was determined according to eq. (49). As aforementioned,

t^{B04}_0 and τ_1-τ_0 were assumed. The specific heat capacity of the unalloyed steel c_p^{B04} was defined as linear function of the temperature, whereat the slope and the absolute coefficient were obtained from 2 pair of values according to [7]. The mass of the tank B04 m^{B04} contains the tank mass itself and the mass of the platform because both components accumulate heat. In contrast the CCFL test rig, the condenser W05 and the pipes inside the pressure tank were not considered since they are sources of heat losses. In this way the heat losses from the CCFL test rig (Q^{tr}) can be estimated in accordance to eq. (42). At this point the authors remind that the aim of the heat losses definition is the correction of the superficial velocity of steam and discharged water from waste condensation effects. Hence the single heat losses were converted to condensation rates:

$$\dot{m}^k_{cond} = \frac{\dot{Q}_k}{(h''_{H2O} - h'_{H2O})}, \text{ for k [N2, N2->B04, W06]} \tag{76}$$

In eq. (76) h_{H2O} is the enthalpy of saturated steam (") and saturated water (') respectively. Both enthalpies were obtained as function of p_{TS}. Then the single condensation rates were summarized to:

$$\dot{m}^\Sigma_{cond} = \dot{m}^{N2}_{cond} + \dot{m}^{N2-B04}_{cond} + \dot{m}^{W06}_{cond} \tag{77}$$

This approach of heat losses estimation applies some simplifications and especially the determination of the heat transfer coefficient by empirical correlations results in uncertainties. To improve the results, a 2nd method was implemented that uses an energy balance over the condenser W05. Thereby the condensate mass flow m^{W05}_{cond} is calculated and subtracted from the injected steam mass flow $m_{G,TS}$ under consideration of the heat losses in the main steam pipe m^{pipe}_{cond}. Hence for the condensate mass flow equivalent of heat losses in the CCFL test rig $m^{tr,W05}_{cond}$ follows:

$$\dot{m}^{tr,W05}_{cond} = \dot{m}_{G,TS} - \dot{m}^{pipe}_{cond} - \dot{m}^{W05}_{cond} \tag{78}$$

Some of the parameter in eq. (78) were already defined: $m_{G,TS}$ by eq. (38) and m^{pipe}_{cond} by eq. (39). The condensate mass flow in W05 was obtained as:

$$\dot{m}^{W05}_{cond} = \dot{m}^{W05}_{cw} \cdot \frac{h^{W05}_{cw,o} - h^{W05}_{cw,i}}{h''_{H2O} - h^{W05}_{cond}}, \tag{79}$$

with m^{W05}_{cw} the cooling water mass flow through the condenser W05, h – enthalpy and the indices: $_{cw}$ for cooling water, $_o$ – outflow, $_i$ – inflow, $_{cond}$ – condensate. The cooling water mass flow is measured by a Coriolis mass flow meter FI8-51 (see Fig. 8). The necessary enthalpies were defined by the water property library as follows:

$$h^{W05}_{cw,o} = f((PI8 - 51), (TI8 - 52)) \tag{80}$$

$$h^{W05}_{cw,i} = f((PI8 - 51), (TI8 - 51)) \tag{81}$$

$$h^{W05}_{cond} = f((PIC8 - 62), (TI8 - 21)) \tag{82}$$

$$h''_{H2O} = f(PIC8 - 62) \tag{83}$$

In this way the heat losses dependent condensate mass flow was defined by eq. (79). A direct measurement of the condensate flow released from W05 is not available. In principle this parameter may be estimated using the level gradient of the condensate drain tank and its cross section area. Due to a discontinuous condensate flow in a gravity pipe, unknown residual condensate content in the condenser W05

and a controlled condensate release to the TOPFLOW blow-off tank the application of this method was refused.

After these evaluations 2 values of heat losses dependent condensate mass flow are available und both methods have their uncertainties. To get an optimal result a weighting function was implemented:

$$\dot{m}_{cond}^{tr} = k_w \cdot \dot{m}_{cond}^{tr,W05} + (1 - k_w) \cdot \dot{m}_{cond}^{\Sigma}, \tag{84}$$

with m_{cond}^{tr} as weighted waste condensation rate and k_w as weighting coefficient. The last one was iterative selected in such a way, that the averaged over all steam tests deviations between the mass gradients of both tanks B19 and B20B, defined according to eq. (28) under consideration of the waste condensation according to eq. (93 and 94), was equal to zero. This condition is complied with $k_w = 0.4$ and hence this value was used for all steam tests. This approach results in a slight overestimation of the waste condensation for the 10 bar tests and to a slight underestimation for the 25 bar and 50 bar tests. Nevertheless the authors think that it is practicable.

Now the entire waste condensation is divided to the single components of the CCFL test rig m_{cond}^k in accordance to their inner surface area relations that had steam contact:

$$\dot{m}_{cond}^{k} = \dot{m}_{cond}^{tr} \cdot \frac{A_{in}^k}{A_{in}^\Sigma}, \text{ for k [B19, TS, B20]} \tag{85}$$

$$A_{in}^\Sigma = \sum_{k=1}^{3} A_{in}^k \tag{86}$$

$$A_{in}^p = 2 \cdot \left(W_{in}^p + L_{in}^p\right) \cdot \left(H_{in}^p - H_{LIC,av}^p\right) + W_{in}^p \cdot L_{in}^p, \text{ for p [B19 and B20]} \tag{87}$$

$$A_{in}^{TS} = \left(2 \cdot H_{in}^{hor} + W_{in}^{hor}\right) \cdot L_{in}^{hor} + L_{in,top}^{incl} \cdot W_{in}^{incl} + 2 \cdot A_{side}^{incl} \tag{88}$$

In eq. (85 – 88) A is the surface area; H, W and L - the height, width and length of the components; indices ^{hor} means horizontal part and ^{incl} inclined part of the test section as well as $_{in}$ for the inner surface. Additional H_{in}^p and $H_{LIC,av}^p$ describes entire height and the time-averaged water level in the tank respectively. Thus the difference results in the steam filled height that is multiplied by the tank circumference. Further the top surface is added. The inner area of the horizontal test section module is obtained by a part of the circumference including twice the channel height and once the width. This value is multiplied by the horizontal channel length. The inclined test section part area is defined by the length of the top contour between both gaps ($L_{in,top}^{incl}$) multiplied by the channel width and the area of both active side windows (A_{side}^{incl}). The last and the contour length were determined by a CAD program. The background of these area calculations is the estimation of the steam contacted area per component. For this reason the bottom parts of the horizontal and inclined module were excluded.

At this point a virtual break is necessary to return to the part (b) of the waste condensation that concerns the heat-up of the discharged water flow in the test section (m_{cond}^{dis}) by the counter current steam flow. The energy balance results to:

$$\dot{m}_{cond}^{dis} = \dot{m}_{B19}^{dis} \cdot \frac{h_{H2O}' - h_{H2O}^{dis}}{h_{H2O}'' - h_{H2O}'}, \tag{89}$$

with m_{B19}^{dis} as discharged water mass flow into the tank B19 and h_{H2O}^{dis} as enthalpy of the discharged water. The first one is calculated by:

$$\dot{m}_{B19}^{dis} = (FIC8^{\cdot} - 42)_{cor} + d\dot{m}_{B19}^{dis}, \tag{90}$$

and the enthalpy results in:

$$h_{H2O}^{dis} = f(p_{TS}, t_{L,TS}^{i}), \tag{91}$$

whereat p_{TS} was calculated according to eq. (34) and $t_{L,TS}^{i}$ with eq. (9).

For some 10 bar tests $t_{L,TS}^{i}$ was higher or equal than t_S due to uncertainties. In these cases h_{H2O}^{dis} and m_{cond}^{dis} were set to zero. The calculation results for this kind of waste condensation are presented at the *Wallis* sheet in the steam Excel files.

Finally the entire waste condensation in the test section was summarized:

$$\dot{m}_{cond}^{TS,\Sigma} = \dot{m}_{cond}^{TS} + \dot{m}_{cond}^{dis} \tag{92}$$

Using the estimated waste condensation rates the mass gradients in both tanks can be corrected:

$$d\dot{m}_{B19}^{dis,cond} = d\dot{m}_{B19}^{dis} - \dot{m}_{cond}^{B19} - \dot{m}_{cond}^{TS,\Sigma} \cdot \frac{(FIC8-42)_{cor}}{(FI8-41)} \tag{93}$$

$$d\dot{m}_{B20B}^{dis,cond} = d\dot{m}_{B20B}^{dis} - \dot{m}_{cond}^{B20B} - \dot{m}_{cond}^{TS,\Sigma} \cdot \frac{(FIC8-40)_{cor}}{(FI8-41)} \tag{94}$$

The single terms in eq. (93 and 94) were obtained as follows: dm_{B19}^{dis} and dm_{B20B}^{dis} in accordance to eq. (13) under consideration of the temperature-dependent volume changing in the tanks and loop parts, m_{cond}^{B19} and m_{cond}^{B20B} according to eq. (85) and $m_{cond}^{TS,\Sigma}$ with eq. (92). $m_{cond}^{TS,\Sigma}$ was weighted by the mass flow ratio as described above.

Further the steam test evaluation procedure of the liquid flow follows the air-water tests. As next steps the deviation between the mass changes of both tanks B19 and B20B was defined according to eq. (28) and the correction of both mass gradients according to eq. (29) was done. Naturally instead of dm_k^{dis} in eq. (29) for steam tests $dm_k^{dis,cond}$ was used. Then the CCFL discharged mass flow using both tanks was obtained by eq. (30) and the averaged value m_{TS}^{dis} was defined by eq. (31). After this the discharged volume flow by eq. (32) and the superficial velocity of the discharged water by eq. (33) were calculated. Finally the non-dimensional liquid superficial velocity according to eq. (2) was defined using the steam and water densities according to eq. (36 and 37).

On the other side the steam mass flow was corrected with the waste condensation rate in the main steam pipe m_{cond}^{pipe}, in the B19 tank m_{cond}^{B19} and $m_{cond}^{TS,\Sigma}$ according to eq. (38, 39, 85 and 92):

$$\dot{m}_{G,TS}^{c} = \dot{m}_{G,TS} - \dot{m}_{cond}^{pipe} - \dot{m}_{cond}^{B19} - \dot{m}_{cond}^{TS,\Sigma}/2 \tag{95}$$

The entire waste condensation in the test section was considered only with 50 % because the counter-current flow limitation proceeded in this module. Using the injected steam mass flow the gas volume flow can be obtained by:

$$\dot{V}_{G,TS} = \frac{\dot{m}_{G,TS}^{c}}{\rho_{G,TS}} \tag{96}$$

Finally the non-dimensional superficial gas velocity was defined according to eq. (6). Despite the complex data evaluation procedure residual uncertainties remain. So the zero penetration points affected with noise and fluctuated around zero. Due to the visual assessment of the complete CCFL condition, j_L^* of the zero penetration tests was set to zero. Similar to the air-water tests also for the steam experiments the

square-roots of the superficial steam and water velocities were plotted to allow a quick look over the test series. The diagram and all calculations were presented at the Excel sheet *Wallis*. After completion of the data evaluation all results were combined in one Excel file, named *HS-II_CCFL_overwiev.xlsx*. This file can be used to compare all CCFL data.

6.3 Evaluation of the pressure sensor data

The installation of 6 pressure sensors on the horizontal module of the hot leg test section was done to determine slug frequencies. Unfortunately the number of pressure proof ducts on the TOPFLOW pressure tank is limited and so the sensors were completely arranged inside the tank. Due to the changing pressure loads most of it busted during operation. Only 2 sensors (PI8-31 and PI8-33, see Fig. 8) kept working until the end of the test series.

Both devices measured pressure sequences with a frequency of 10 Hz for 60 seconds for each test. After check of the data it was decided to use a Fast Fourier Transformation to analyze it and to detect significant slug frequencies. For this the common files of the data logger (see section 5.3 Data of the special pressure sensors) were reduced to the valid data channels and to the relevant period and stored as "*common test name*.txt" files. Then they were analyzed by a FFT routine that generates data files ("*common test name*.fft.txt"). These files contain 3 columns: the detected frequencies and the rate of occurrence for both sensors.
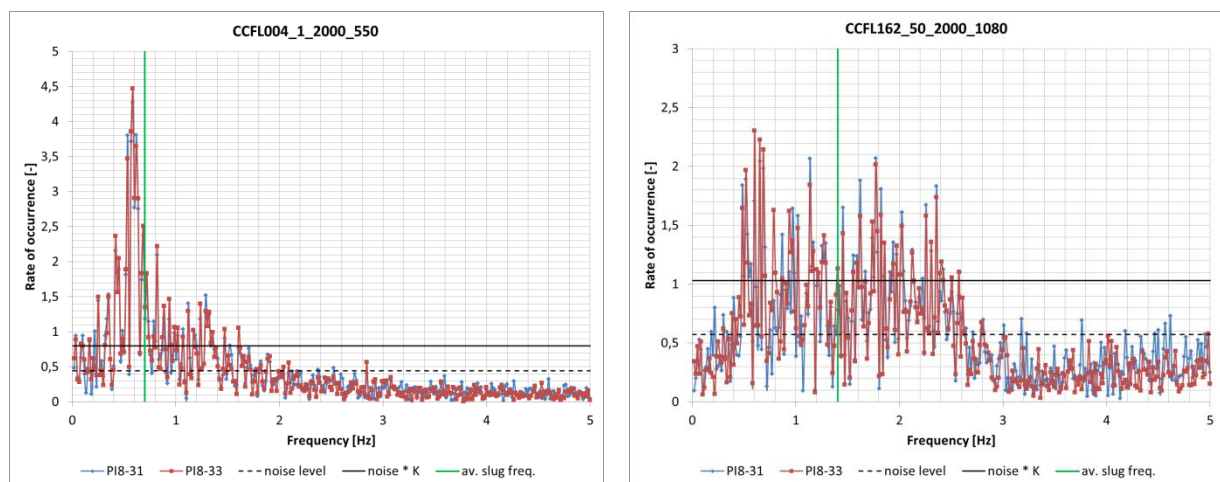

Fig. 14 FFT data for two selected hot leg tests: left side – air water test 004 at 1 bar pressure and 557 nm³/h gas flow; right side – steam water test 162 at 50 bar pressure and 1050 g/s steam mass flow; both tests with 2 kg/s injected water mass flow

Fig. 14 shows 2 plots of characteristic FFT-pattern. At the left side a clear spectrum is visible. In this case the maximum rate of occurrence represents the most probably frequency, whereat some further maxima exist. In opposite the right graphic shows a much more expanded spectrum. Here the maximum rate of occurrence results in a random frequency. Unfortunately most of the FFT data belong to the second class. So a weighted averaging method was applied. Firstly a virtual noise level (L_N) was obtained:

$$L_N = \frac{\sum_{i=1}^{n} RO}{n} \tag{97}$$

In eq. (97) RO stands for rate of occurrence and n is the number of all FFT-values. In Fig. 14 this level is visualized by the black dotted horizontal line. Now for all FFT-

values which RO is higher than the noise level a weighted average frequency was defined:

$$F_{av} = \frac{\sum_{i=min}^{max} F_i \cdot RO_i}{\sum_{i=min}^{max} RO_i}$$ (98)

Eq. (98) contains: F as frequency and the indices av – for averaged value, min as minimal FFT frequency which RO >= the noise level and max – the maximal value respectively. A first analysis of the results revealed, that artificial effects influenced the averaged frequencies due to the wide available frequency sector. For this reason a factor (k) was introduced that increases the virtual noise level.

$$L_k = k \cdot L_N$$ (99)

To estimate the influence of k a parameter study was done. For a first rough analysis, values between 1 and 3 with a step of 0.5 were applied. The weighted frequency as function of k was calculated and compared for each CCFL test sorted by test series (constant pressure and injected water mass flow). As result of the rough analysis k was found in a range of 1.5 to 2. As selection criterion the frequency curves as function of k and the test points of each series was checked. The factor k was chosen in such a way, that the frequency curves showed a smooth characteristic without strong outliers. To improve the factor, a 2nd parameter study was conducted between 1.5 and 2 with a step of 0.1. Finally 1.8 was found as a good compromise for the entire CCFL test data and this value was used for the further data evaluation. The increased level (L_k) is plotted at the graphs in Fig. 14 as solid black line. The weighted frequency for k = 1.8 was obtained by eq. (98) and is shown in both graphs as green vertical line. Then the slug frequencies for all CCFL tests were analyzed as function of the real gas volume flow and in dependence of the gas mass flow.

6.4 Analysis of the optical observation data

As aforementioned a high-speed camera was installed in the pressure tank to capture picture sequences of the counter-current flow in the inclined module of the CCFL test section. So after completion of the measurements picture sequences of 13 s with a frequency of 500 Hz are available. These images enable a detailed investigation of the flow structure and so they were used for an optical analysis of the slug frequencies and of the flow morphology.

Two web cams were used to observe the horizontal part of the hot leg model. Their videos were used to detect the zero penetration condition of the CCFL flow. In addition selected high speed images and single pictures of the video sequences can be mounted together to get a synchronized flow visualization of the entire CCFL test section.

7. Results

7.1 Investigation of the flooding characteristics

In the previous section the evaluation procedures of the operational data were described very detailed. They result in non-dimensional gas (j_G*) and discharged liquid (j_L*) superficial velocities which square roots were visualized.
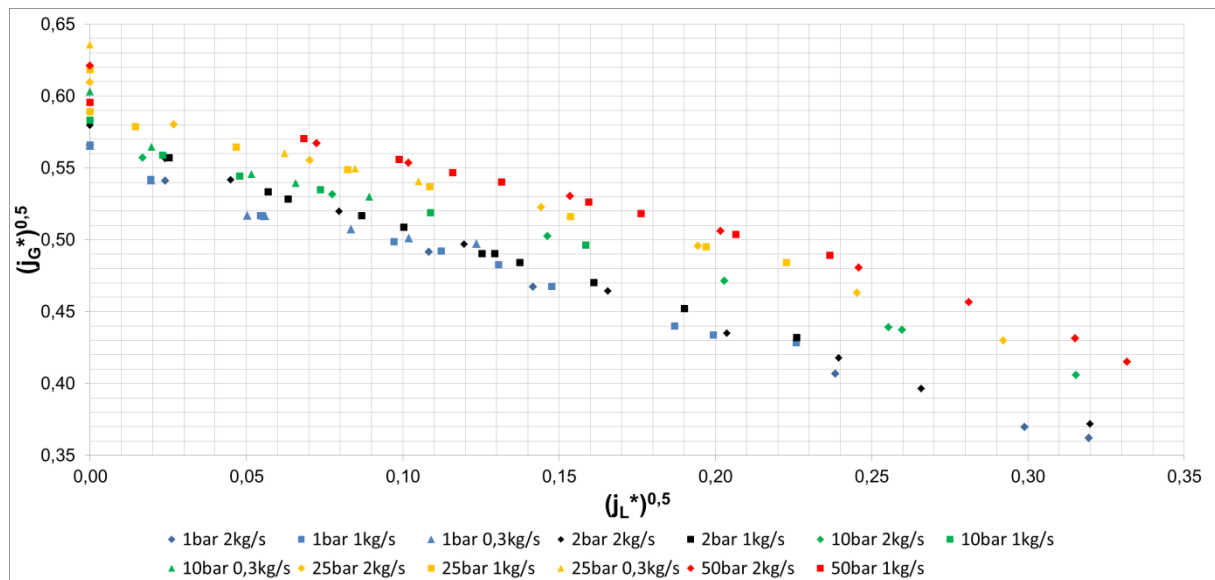

Fig. 15 Flooding characteristics of the hot leg model plotted in terms of Wallis parameter

Fig. 15 presents all CCFL data sorted by the thermal hydraulic boundary conditions. It displays the tests of the flooding and deflooding process that are arranged at the same line. The air-water tests at 1 bar marked with blue and the 2 bar tests with black symbols. For the visualization of the steam-water results the following colors were used: 10 bar: green, 25 bar: yellow and 50 bar: red. Further the rhombs mark the tests with 2 kg/s water injection, the quadrats – 1 kg/s and the triangles – 0.3 kg/s respectively. So the graph shows the tests arranged by series. It is clearly visible, that for the single series, started with 1 bar air tests, the non-dimensional gas superficial velocity increases with increasing pressure for constant discharged liquid flow. Furthermore the test points form almost lines for each pressure, independent of the injected water mass flow. For a further analysis of the linearly dependence the curves of the single series were investigated in detail. Due to the fact, that the test points with zero discharged liquid flow have mostly an increased gas flow (more than theoretical necessary), these points are eliminated from the linearity check. Fig. 16 exemplary shows the data for all three 10 bar steam water test series with linear fits on the left side and quadratic approximation on the right side for the 2 kg/s series. Similar to these graphs all data were processed and the results entered in Tab. 3. Beside the pressure and the injected liquid mass flow it contains the parameters of the fitting procedure: P2 as quadratic, P1 as linear and P0 as absolute coefficient. P2 only exists for the 2 kg/s series because only in this case and only for the steam tests a quadratic approximation results in a significant improvement of the fit, e.g in a significant reduction of the coefficient of determination (R^2). For the other experiments the test points are arranged more or less in a stochastic way. Hence the linear fit seems sufficient.
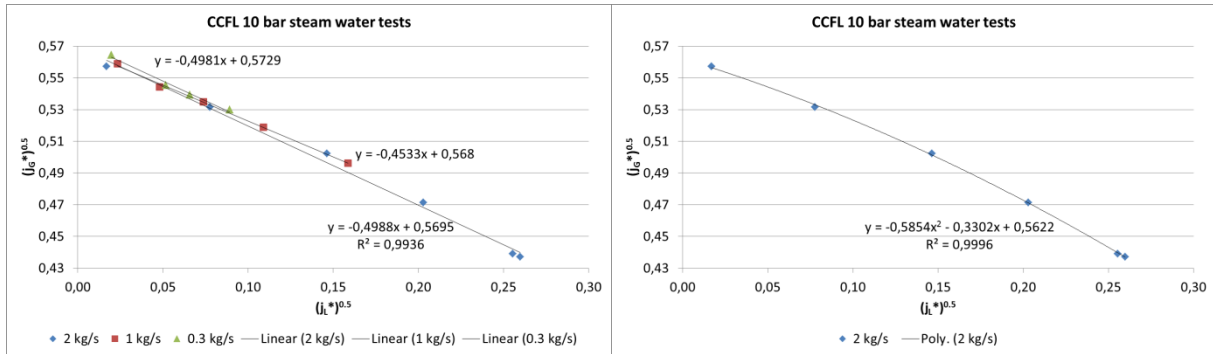
Fig. 16 Analysis of the flooding characteristics for the 10 bar tests; left hand side: 3 series for all injected liquid mass flows with linear fits; right hand side: quadratic approximation of the 2 kg/s series

Tab. 3 Parameter of the flooding curve analysis

Pressure [bar]	Injected liquid mass flow [kg/s]	P2	P1	P0	R^2
1	2		-0.6074	0.5522	0.9965
		-0.1273	-0.5666	0.5502	0.9967
1	1		-0.5821	0.5526	
1	0.3		-0.4660	0.5455	
2	2		-0.6565	0.5703	0.9987
		-0.0874	-0.6313	0.5711	0.9987
2	1		-0.6244	0.5703	
10	2		-0.4988	0.5695	0.9936
		-0.5854	-0.3302	0.5622	0.9996
10	1		-0.4533	0.5680	
10	0.3		-0.4981	0.5729	
25	2		-0.5518	0.5972	0.9929
		-0.5555	-0.3765	0.5882	0.9985
25	1		-0.4572	0.5860	
25	0.3		-0.4511	0.5878	
50	2		-0.5751	0.6150	0.9882
		-0.8817	-0.2164	0.5859	0.9993
50	1		-0.4816	0.6031	

Furthermore the slope (P1) of the linear fits was analyzed. Thereby the tests with 0.3 kg/s were excluded because only a few points are available and additionally they are arranged in a narrow sector. Hence the slope uncertainty is higher than for the other tests. So it was found that at constant pressures the slope slightly increases with decreasing injected liquid mass flow. Thereby it is important that P1 for the quadratic fit has to be ignored. The comparison of the slopes between the different pressures under consideration of constant injected liquid mass flow results also in a

monotonous behavior. The values decrease with increasing pressure but from different starting levels (-0.61 – air and -0.5 – steam).
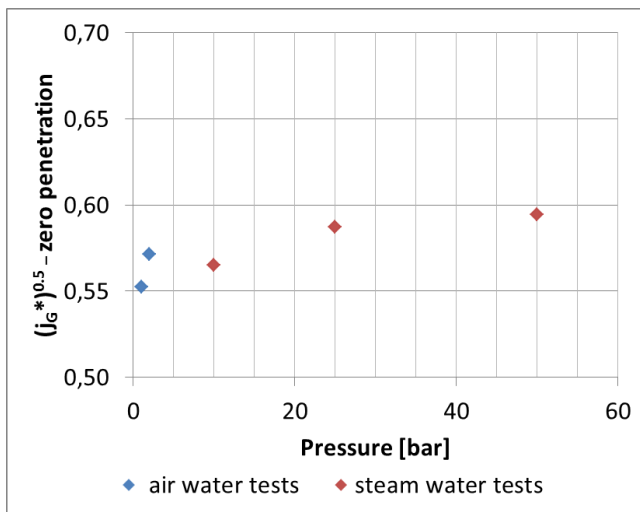

Fig. 17 Plot of the calculated zero penetration points as function of the pressure

The next step was the analysis of the absolute coefficient P0 that represents the intersection with the ordinate. In case of the flooding characteristics this point is the calculated zero penetration value. The accuracy of this parameter depends on the number and on the range of the data. So also for this analysis the 0.3 kg/s series were excluded. The other 2 values at constant pressure are almost equally, so they were averaged. Additional is noted that for the 2 kg/s steam tests P0 from the quadratic approximation was used.

Taking these conditions into account, the calculated zero penetration points slightly increase with increasing pressure, if we observe air and steam individual. Now the calculated zero points were compared with the measured values around zero penetration condition (see also Fig. 18). Except the test series 2 bar and 1 kg/s were zero condition was not achieved, all other series satisfy the condition that the experimental zero V_G was higher or equal than the calculated values and also the experimental CCFL points near zero condition are completely lower than the calculated zero value. So a 2nd way for the verification of zero penetration condition was identified, in addition to the visual observation.

Another interesting feature of the CCFL tests results from a closer look to the test matrixes in Tab. 1 and Tab. 2 in addition with the experimental procedure. Fig. 18 shows all CCFL test series started from the counter-current flow, down to zero penetration condition and back to the CCF. It is clearly visible that for all series the CCFL starts at higher gas volume flows as it breaks down, it means that there is a hysteresis between CCFL start and end condition. The width of this hysteresis depends on the injected water mass flow, as higher the water flow as wider the hysteresis. This fact is easy to understand, because as higher the injected water mass flow as more liquid is available above the inclined test section module and can feed the discharge water flow. Furthermore it is obviously, that the CCFL starts at significant lower gas flows for the 1 kg/s test series and hence the difference between the gas flows at CCFL start condition and zero penetration point in these cases is much higher. This effect is also highlighted in the test matrixes, where the zero penetration points are arranged at one horizontal line.
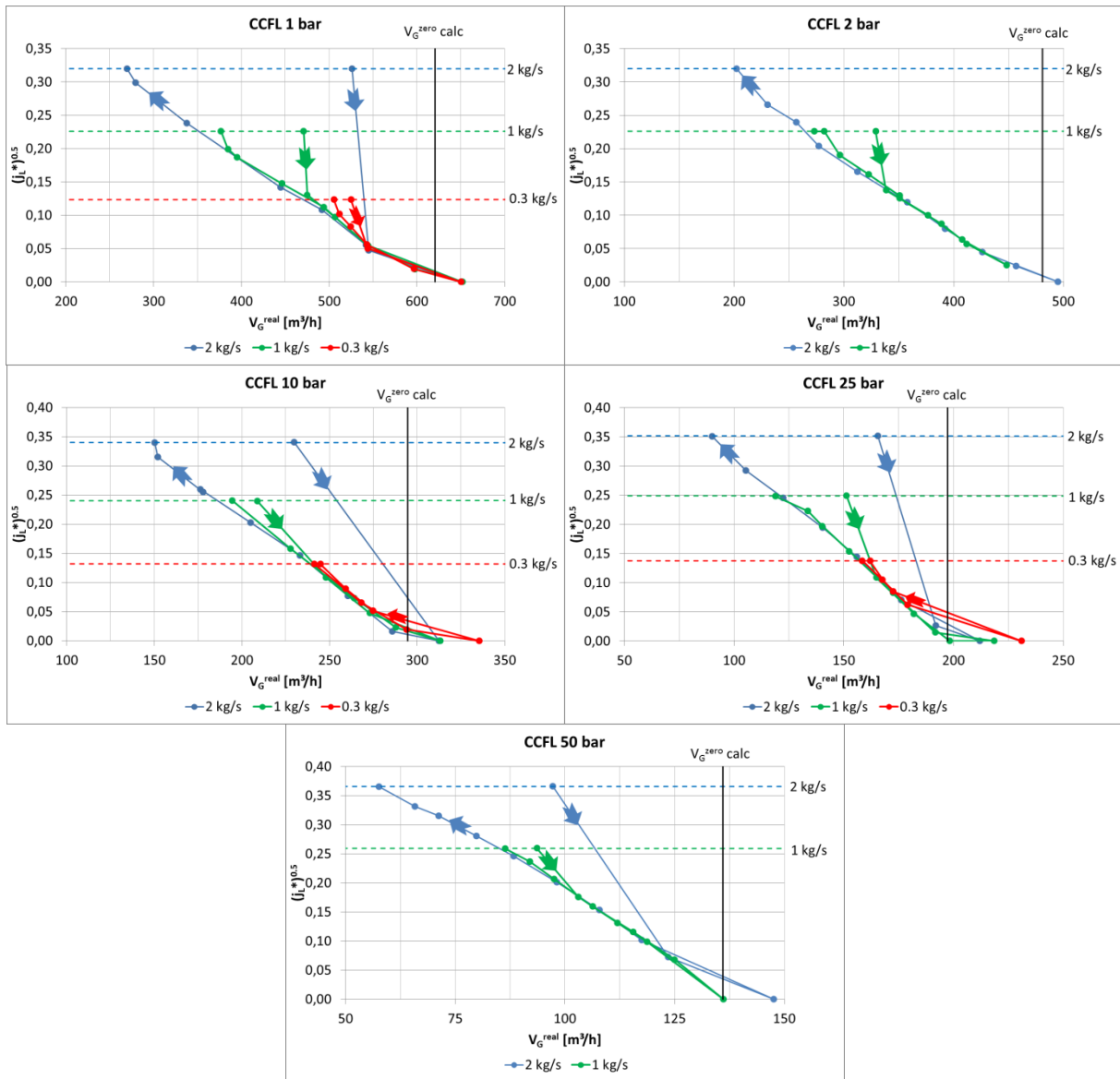
Fig. 18 Visualization of the CCFL test series development sorted by pressure and injected water mass flow

7.2 Analysis of the slug frequencies

Beside the operational data also pressure measurements on the horizontal test section module are available. The evaluation procedure for the pressure data was described in section 6.3 Evaluation of the pressure sensor data. If this procedure is applied for all test points where slugs appeared (excluding CCF), it results in averaged slug frequencies for each test point which are plotted at Fig. 19. For clarity the points are also arranged by test series and labeled by the same symbols and colors similar to Fig. 15. The visualization of the slug frequencies reveals two clear trends: On the one hand it is obvious, that the slug frequency increase with increasing pressure. For a quantitative analysis the single slug frequencies of each test series were averaged. Fig. 20 displays 3 curves arranged by the injected water mass flow. On the other hand the slug frequency decreases with increasing injected water mass flow, if the pressure is kept constant. This effect is shown at Fig. 21.
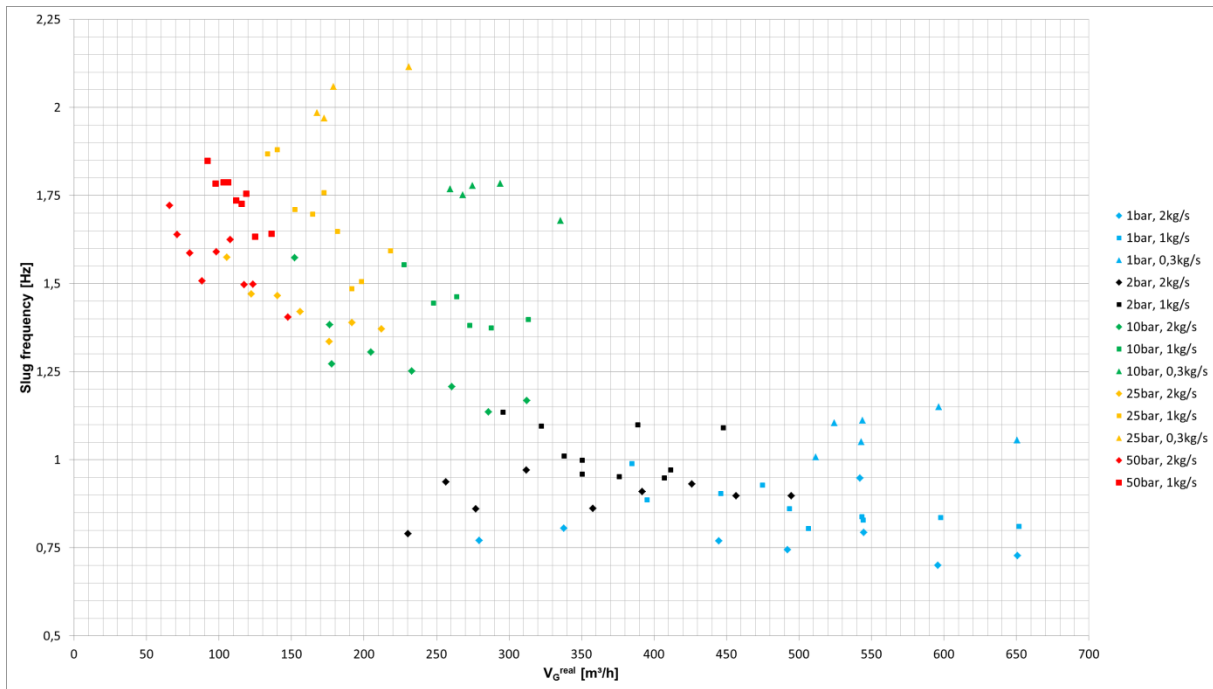
59

Fig. 19 Visualization of the averaged slug frequencies as function of the real gas
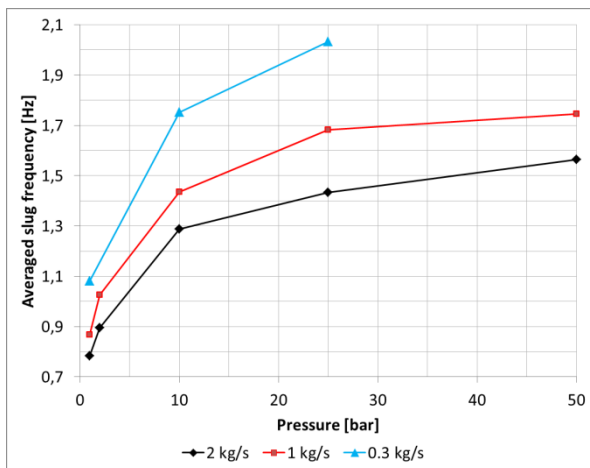volume flow, sorted by test series

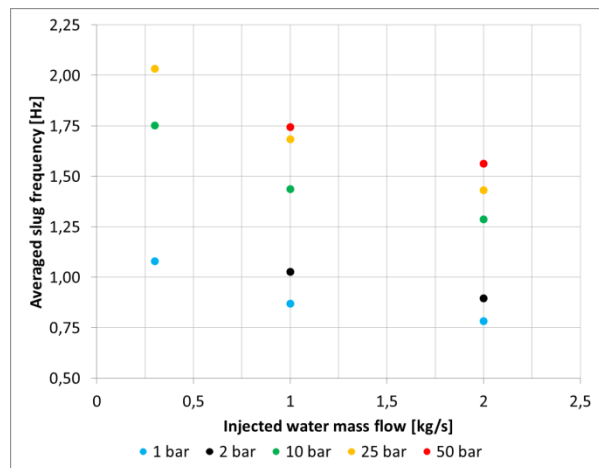Fig. 20 Slug frequencies as a function of
pressure

Fig. 21 Slug frequencies subject to the
injected water mass flow

For some pressure levels the slug frequency slightly decreases with increasing gas flow. This effect is visible for 10 bar (2, 1 and 0.3 kg/s), for 25 bar (2 and 1 kg/s) and for 50 bar (2 and 1 kg/s). However the air test series and the 25 bar 0.3 kg/s test series doesn't follow this trend. In consideration of the wide frequency spectrum over the single tests this effect may be inside the measurement and evaluation uncertainty.

7.3 Optical observation

The very extensive video material was used as a second way of slug frequency detection. Therefore all high speed camera images were displayed in successive order and if a slug appeared the image number was noted. This process results in a list of slug image numbers that was converted in slug frequencies using the image capture frequency. Unfortunately the outcome was not as good as the numerical FFT

evaluation. The clear trends of the slug frequency development according to the pressure and the injected water mass flow couldn't be confirmed by this optical method. Nevertheless the inspection of the image sequences reveals to a better understanding of the flow morphology in the horizontal and inclined test section parts.

The measurement series always starts from counter-current flow condition. It means that the water injected into the SG separator flows unhindered through the test section into the RPV simulator with a smooth interface between gas and liquid. Then the gas flow was increased and the counter-current water flow was limited. This process started in the horizontal test section part. The flow was wavier with an increasing level in the horizontal part from the RPV side to the SG side. Near the transition to the inclined part first slugs appeared, but they didn't touch the top wall. A further increase of the gas flow led to an intensification of the water obstruction and to a rise of the slug level up to the top wall. The gas flow pushed the slugs into the inclined part and further over the steel sheet between B20A and B20B. In this way the discharge water flow decreased down to zero, if the gas flow is high enough. During zero penetration the horizontal channel on the RPV side is partly waterless, at which the border moves along the RPV faced horizontal channel module. A decreasing gas flow led to a reverse process with a hydraulic jump that moved from the RPV faced horizontal channel into the inclined module.

During CCFL different kinds of slugs appeared: There are flows with almost single slugs, double and even multiple slugs. A good example for a flow with almost single slugs is the test CCFL004 which frequency spectrum was shown at Fig. 14 left side. In this case the time between two successive slugs is almost constant (around 1.4 s). In contrast flows with double or even multiple slugs have a wide frequency spectrum. The test 162 (Fig. 14, right side) is a good example for the frequency spectrum of this kind of flow. Fig. 22 shows a representative example of multiple slugs of the air water test 026 with a distance between two slugs of 0.23 s.
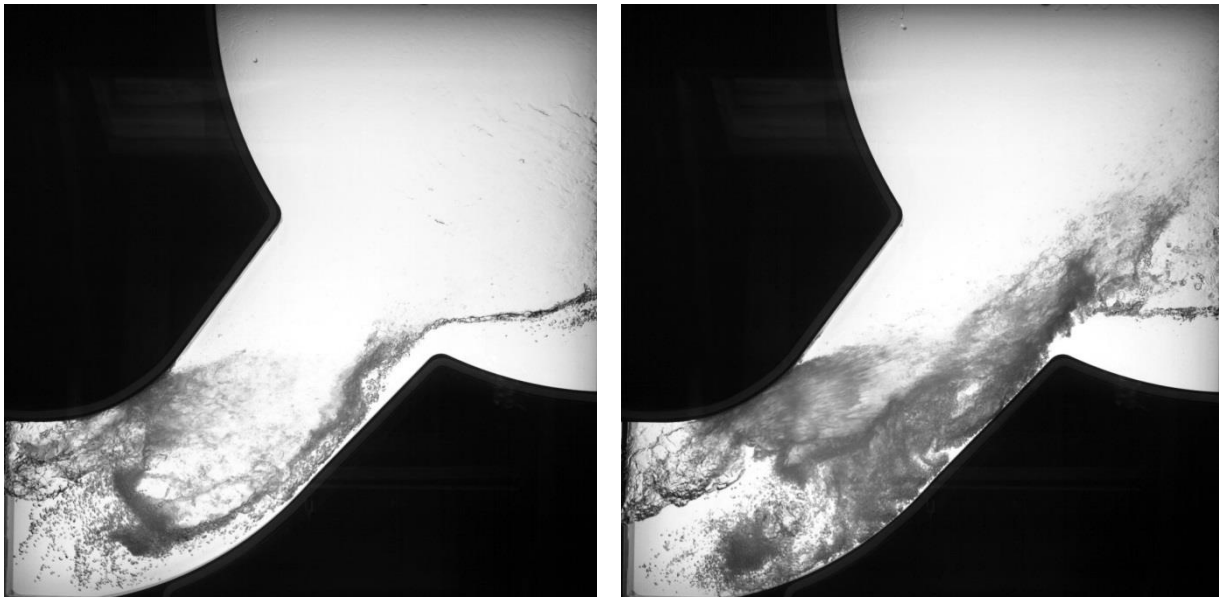

Fig. 22 Example of a double slug with a time delay of 0.23 s; left side - picture 1750 and right side – picture 1865 of the test 026

Multiple slugs appeared mostly if the water flow in the inclined test section module began to rotate driven by the gas flow. Thereby the water of the primary slug remained in the bottom part of the inclined module and was available for the next

61

slug, which very fast can rise and obstruct the channel. For further investigation of slug morphology the authors refer to the image sequences.

8. Summary and outlook

The present report describes the 2015 series of the so called hot leg tests. The hot leg is a component of a PWR primary circuitry and the technical need of its scientific investigation occurs from a leakage flow accident scenario, more precisely from the expectable cooling power of the residual heat during such an accident. A new series with special focus to the counter-current flow limitation was desired since from the results of the previous test series some ideas for improvements were born, especially concerning the experimental procedure and test section design. Also in the field of optical observation the measurement possibilities were significant improved. As the previous test rig also the current experimental set-up was operated in the TOPFLOW pressure tank that allows combining high pressure tests with large-scale observation thanks pressure equilibrium. Thereby a new developed thermal insulation technology was successfully applied. A further improvement results from the operation of the circulation loops that allows the use of mass balances for the data evaluation.

The reconstruction and preparation of the test rig were finished in May 2015. Then extensive air-water tests at 1 and 2 bar as well as steam/saturated water tests at 10, 25 and 50 bar followed until the end of June in the same year. They result in app. 100 operational parameters which were stored with a frequency of 1 Hz during the test time of one minute with a preliminary time span of approximately 10 minutes. Additional the flow structure was observed by a high speed camera (inclined test section module) with a frequency of 500 Hz over 13 s and by 2 web cameras (horizontal channel) with a frequency of about 60 Hz as video recording during the test time. Finally pressure data with 10 Hz over the test time are available from the horizontal channel.

After completion of the measurements the database was used to calculate flooding characteristics in term of Wallis parameter. A detailed analysis of these flooding lines reveals a slight parallel shift between it in dependence on the pressure. Also a slight decreasing of the slope at increasing pressure was found. In addition the hysteresis between start and breakdown of the counter-current flow limitation and the real zero penetration point was investigated. Beside the flooding characteristics slug frequencies were obtained. This parameter shows a clear dependence on the pressure and on the injected water mass flow.

As next steps it would be very useful to develop a correction term that eliminates the parallel pressure-dependent shift of the flooding characteristics. Here the kinematic viscosity could be an interesting parameter. Also the development of a correlation for the slug frequencies seems possible with the available data. For the enhancement of the new CFD-based models, like AIAD or GENTOP, the evaluation of the image and video data may contribute in a significant way. Especially the detection of the interfacial area by digital image processing or phase velocity determination by tracking algorithms is possible with the high-resolution and frequency image sequences.

Literature

[1]   Seidel, T., Vallee, C., Lucas, D., Beyer, M., Deendarlianto (2011). Two-phase flow experiments in a model of the hot leg of a pressurized thermal reactor. Helmholtz-Zentrum Dresden-Rossendorf, technical report, HZDR-010, September 2011, ISSN 2191-8716

[2]   Wallis, G. B. & Dobson, J. E. (1973). The onset of slugging in horizontal stratified air-water flow. International Journal of Multiphase Flow 1, pp. 173 – 193

[3]   Hihara, E., Soejima, H., Saito, T. (1985). Slugging of countercurrent gas–liquid flow in a horizontal channel. Nippon Kikai Gakkai Ronbunshu (B) 51, 394–397

[4]   Zapke, A., Kröger, D.G. (2000). Counter-current gas–liquid flow in inclined and vertical ducts; Flow patterns, pressure drop characteristics and flooding. International Journal of Multiphase Flow 26, 1439–1455

[5]   Deendarlianto, Vallée, C., Lucas, D., Beyer, M., Pietruske, H., Carl, H. (2008). Experimental study on the air/water counter-current flow limitation in a model of the hot leg of a pressurized water reactor. Nuclear Engineering and Design 238, pp. 3389 – 3402

[6]   VDI Wärmeatlas – Berechnungsblätter für den Wärmeübergang, Herausgeber: Verein Deutscher Ingenieure – 7. Erweiterte Auflage, Düsseldorf, VDI Verlag, 1994

[7]   VDI Wärmeatlas, Herausgeber: Verein Deutscher Ingenieure – 11. Erweiterte Auflage, Springer Verlag Berlin Heidelberg 2013